JAEA-Data/Code
2014-001

Property Database of TRU Nitride Fuel

Tsuyoshi NISHI, Yasuo ARAI, Masahide TAKANO and Masaki KURATA

Division of Fuels and Materials Engineering
Nuclear Science and Engineering Directorate

March 2014

Japan Atomic Energy Agency

日本原子力研究開発機構

JAEA-Data/Code

本レポートは独立行政法人日本原子力研究開発機構が不定期に発行する成果報告書です。
本レポートの入手並びに著作権利用に関するお問い合わせは、下記あてにお問い合わせ下さい。
なお、本レポートの全文は日本原子力研究開発機構ホームページ（http://www.jaea.go.jp）
より発信されています。

独立行政法人日本原子力研究開発機構　研究技術情報部　研究技術情報課
〒319-1195　茨城県那珂郡東海村白方白根 2 番地 4
電話 029-282-6387, Fax 029-282-5920, E-mail:ird-support@jaea.go.jp

This report is issued irregularly by Japan Atomic Energy Agency.
Inquiries about availability and/or copyright of this report should be addressed to
Intellectual Resources Section, Intellectual Resources Department,
Japan Atomic Energy Agency.
2-4 Shirakata Shirane, Tokai-mura, Naka-gun, Ibaraki-ken 319-1195 Japan
Tel +81-29-282-6387, Fax +81-29-282-5920, E-mail:ird-support@jaea.go.jp

JAEA-Data/Code 2014-001

Property Database of TRU Nitride Fuel

Tsuyoshi NISHI, Yasuo ARAI, Masahide TAKANO and Masaki KURATA

Division of Fuels and Materials Engineering, Nuclear Science and Engineering Directorate,
Japan Atomic Energy Agency
Tokai-mura, Naka-gun, Ibaraki-ken

(Received January 9, 2014)

The purpose of this study is to prepare a property database of nitride fuel needed for the fuel design of accelerator-driven system (ADS) for transmutation of minor actinide (MA). Nitride fuel of ADS is characterized by high content of Pu and MA as principal components, and addition of a diluent material such as ZrN. Experimental data or evaluated values from the raw data on properties Pu and MA nitrides, and nitride solid solutions containing ZrN are collected and summarized, which cover the properties needed for the fuel design of ADS. They are expressed as an equation as much as possible for corresponding to a variety conditions. Error evaluation is also made as much as possible. Since property data on transuranium (TRU) nitrides are often lacking, those on UN and (U,Pu)N are substitutionally shown in such cases in order to facilitate the fuel design with a tolerable accuracy by complementing the database.

Keywords: Property Database, Transuranium (TRU), Nitride Fuel, Accelerator-driven System (ADS), Transmutation, Minor Actinide (MA), ZrN

JAEA-Data/Code 2014-001

TRU 窒化物燃料物性データベース

日本原子力研究開発機構　原子力基礎工学研究部門　燃料・材料工学ユニット
西 剛史、荒井 康夫、高野 公秀、倉田 正輝

(2014 年 1 月 9 日　受理)

本研究の目的はマイナーアクチノイド（MA）核変換用加速器駆動システム（ADS）の燃料設計に必要な窒化物燃料の物性データベースを整備することである。ADS 用の窒化物燃料には Pu 及び MA が主要成分として含まれること、ならびに ZrN 等の希釈材が添加されることに特徴がある。このため Pu や MA の窒化物のほか ZrN を含む窒化物固溶体を対象として、ADS の燃料設計に必要な物性に関する実験値や評価値を収集・整理した。これらの物性値は設計において種々の条件に対応しやすくするため、可能な限り定式化することに努めた。また、誤差の推定が可能な物性値についてはその評価結果も記載した。Pu や MA 等の超ウラン元素（TRU）窒化物については実験値や評価値が報告されていない物性値も多いので、その場合は代替として UN や(U,Pu)N の報告されている物性値でデータベースを補完することにより、許容できる精度を持った ADS 燃料の設計ができるようにした。

原子力科学研究所（駐在）：〒319-1195　茨城県那珂郡東海村白方白根 2-4

Contents

目　次

List of Tables

List of Figures

1. Introduction

Nitride fuel has been developed since 1970s mainly in USA, Europe, Russia, India and Japan; it was proposed as an advance fuel for fast reactor [1], space reactor [2] and accelerator-driven system (ADS) for the transmutation of minor actinides (MA; Np, Am, Cm) [3]. Further, recently UN has attracted attention as a candidate of the accident-tolerant fuels (ATF) of light water reactor that meets highly resistance to oxidation and fission products release under beyond-design-basis accident conditions [4]. Although the number of property data sets of nitride fuel is limited in comparison with that of oxide fuel or metallic fuel, the marginal data of UN and (U,Pu)N needed for the design of fast reactor and space reactor are available. On the other hand, the efforts on nitride fuel development for recent 10 years in Japan Atomic Energy Agency (JAEA) focus on the preparation and property measurements of transuranium (TRU) nitrides. In this case TRU nitrides represent not only Pu nitride, minor actinide (MA; Np, Am, Cm) nitride and their solid solution, but also the solid solution of TRU nitride and ZrN that is proposed for the fuel of ADS [3]. Typical composition of nitride fuel for ADS proposed by JAEA is the solid solution of $(MA_{0.14\text{-}0.16}Pu_{0.10\text{-}0.12}Zr_{0.73\text{-}0.75})N$ with highly ^{15}N-enriched nitrogen. Recently, TRU nitride diluted by TiN is also proposed for the fuel of ADS alternatively, although a lot of technical issues for the preparation remain [5]. The purpose of this study is to prepare a property database of TRU nitrides, in which their properties needed for the design of ADS are covered.

The relation of fuel design, irradiation behavior and property data collected and estimated in this study is illustrated in Fig. 1. Basic design parameters, such as the dimension, power density, target burnup, temperature distribution and safety margin of the fuel is determined from the fuel properties themselves and the irradiation behavior at burnup progressing. The irradiation behavior affecting the design parameters includes the change of gap conductance, crack and relocation, restructuring, Fuel-Cladding Chemical Interaction (FCCI), Fuel-Cladding Mechanical Interaction (FCMI) and so on. They are caused by the temperature gradient in the fuel pellet, internal pressure of the fuel element, and chemical and mechanical stresses subjected to the cladding tube, which are mostly governed by the properties of fuel, cladding and bonding materials in addition to the irradiation condition.

Collected experimental data or evaluated values from the raw data on TRU nitrides in this study include the molecular weight, lattice parameter and theoretical density, heat capacity, thermal conductivity, thermal expansion, electrical resistivity and magnetic properties, melting temperature and decomposition pressure, vapor pressure, Gibbs free energy of formation, thermodynamic functions, mechanical properties, diffusion characteristics, fission gas release and swelling characteristics. These properties are

expressed as an equation as much as possible for corresponding to a variety of conditions. Error evaluation is also made as much as possible. Accordingly, a practical fuel design of ADS has become feasible. Further, the effects of the sample characteristics, such as grain size and porosity, on properties are considered in some equations because they can change the properties as large as ± 50 % in several cases.

Since property data on TRU nitrides are often lacking, those on UN and (U,Pu)N are substitutionally shown in such cases in order to facilitate the design of ADS with a tolerable accuracy by complementing the present database. Those on UN are mostly cited from the efforts in USA [6-11], in which UN had been developed as a potential fuel for space reactor in "SP-100 Program" [2]. On the other hand, those on (U,Pu)N are mostly cited from two distinguished monographs by Matzke [1] and Blank [12] of Institute for Transuranium Elements (ITU), in which (U,Pu)N as well as (U,Pu)C had been investigated as an advance fuel for fast reactors in detail. Moreover, a few property data on TRU nitrides are cited from the reports of the Advanced Accelerator Assisted (AAA) and the Advance Fuel Cycle Initiative (AFCI) programs of USA [13,14]. Thermodynamic and thermophysical data of actinide nitrides recently compiled in "Comprehensive Nuclear Materials" [15] are also cited.

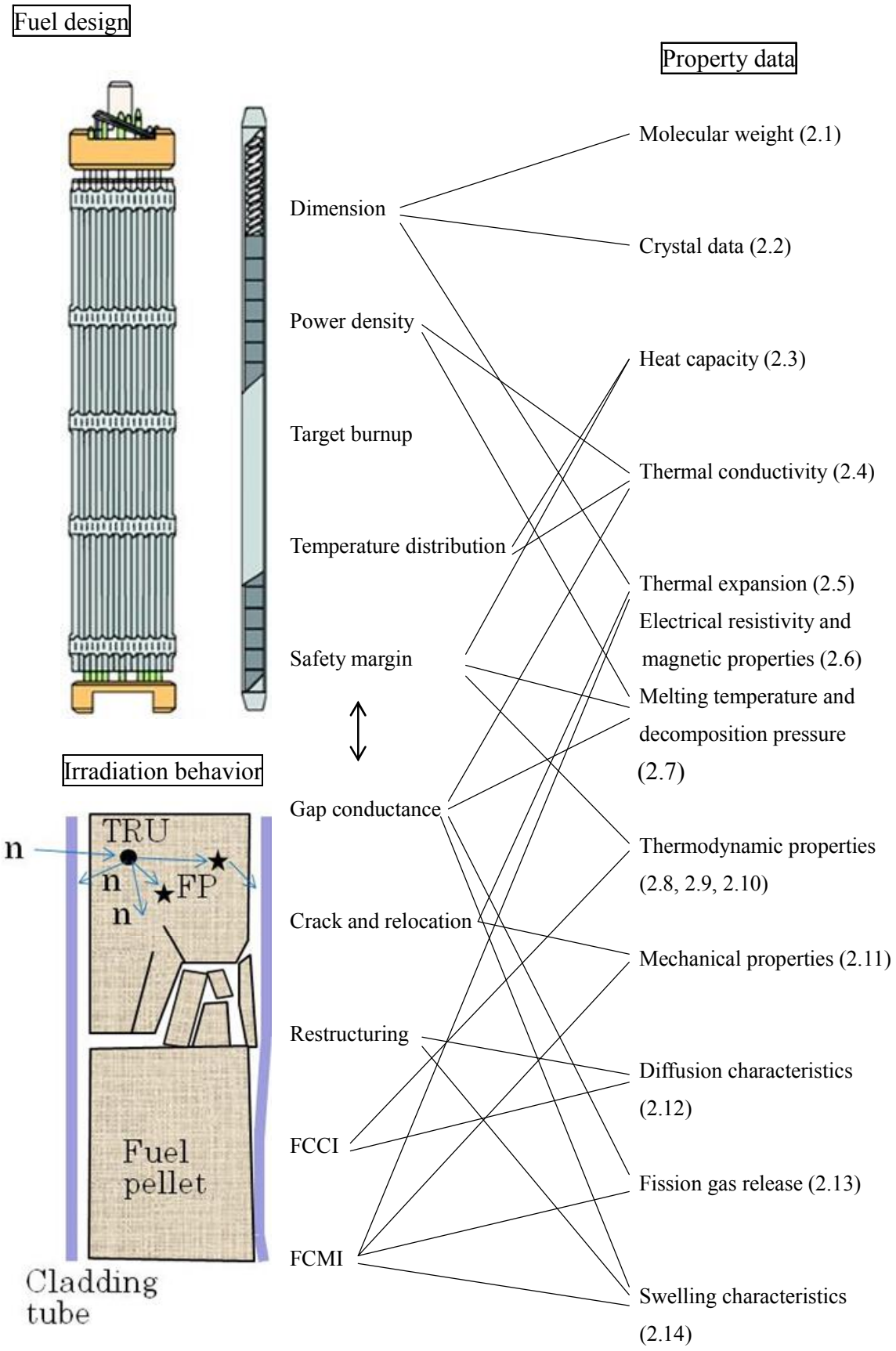

Fig. 1 Relationship between fuel design, irradiation behavior and property database

2. Property database of TRU nitride fuel

2.1 Molecular weight

2.1.1 Molecular weights of UN, NpN, PuN, AmN, CmN and (Zr,Np,Pu,Am,Cm)N

Molecular weights of UN, NpN, PuN, AmN and CmN are listed in Table 2-1-1, in which atomic weights of U, Np, Pu, Am, Cm and natural N (M_U, M_{Np}, M_{Pu}, M_{Am}, M_{Cm} and M_N) are assumed to be 238.03, 237, 239.26, 241, 244 and 14.01, respectively.

Table 2-1-1 Molecular weights of UN, NpN, PuN, AmN and CmN

Material	UN	NpN	PuN	AmN	CmN
M	252.04	251.01	253.27	255.01	258.01

On the other hand, molecular weight of $(Zr_{1-w-x-y-z}Np_wPu_xAm_yCm_z)N$ is calculated from the following equation, in which atomic weight of Zr (M_{Zr}) is assumed to be 91.22.

$$M = (1-w-x-y-z)\,M_{Zr} + w\,M_{Np} + x\,M_{Pu} + y\,M_{Am} + z\,M_{Cm} + M_N$$
$$= 105.23 + 145.78\,w + 148.04\,x + 149.78\,y + 152.78\,z \qquad (2\text{-}1\text{-}1)$$

Fig. 2-1-1 shows the composition dependence of molecular weight of $(Zr_{1-2x}Pu_xAm_x)N$ solid solution calculated from Eq. (2-1-1).

In case N-15 enriched nitrogen to 99.9% is used, molecular weights of $U^{15}N$, $Np^{15}N$, $Pu^{15}N$, $Am^{15}N$ and $Cm^{15}N$ are listed in Table 2-1-2.

Table 2-1-2 Molecular weights of $U^{15}N$, $Np^{15}N$, $Pu^{15}N$, $Am^{15}N$ and $Cm^{15}N$

Material	UN	NpN	PuN	AmN	CmN
M	253.03	252.00	254.26	256.00	259.00

Similarly, molecular weight of $(Zr_{1-w-x-y-z}Np_wPu_xAm_yCm_z)^{15}N$ is calculated from the following equation.

$$M = 106.22 + 145.78\,w + 148.04\,x + 149.78\,y + 152.78\,z \qquad (2\text{-}1\text{-}2)$$

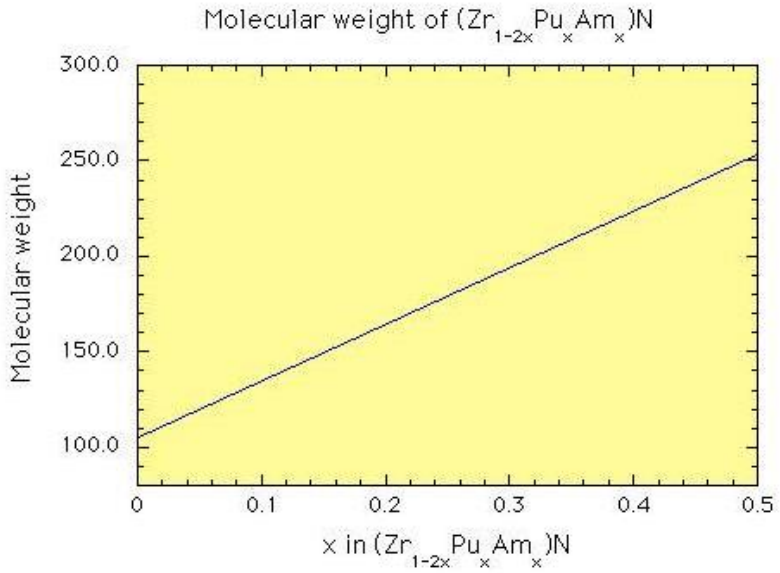

Fig. 2-1-1 Molecular weight of $(Zr_{1-2x}Pu_xAm_x)N$ with natural nitrogen

2.2 Lattice parameter and theoretical density

2.2.1 Lattice parameter of UN, NpN, PuN, AmN and CmN

Lattice parameters of UN, NpN, PuN, AmN and CmN summarized by Benedict [16] are shown in Table 2-1-1 and Fig. 2-2-1. The uncertainty is less than ± 0.001 nm.

Table 2-2-1 Lattice parameters of UN, NpN, PuN, AmN and CmN

	UN	NpN	PuN	AmN	CmN
Lattice parameter (nm)	0.48887	0.48987	0.4905	0.4995	0.5027

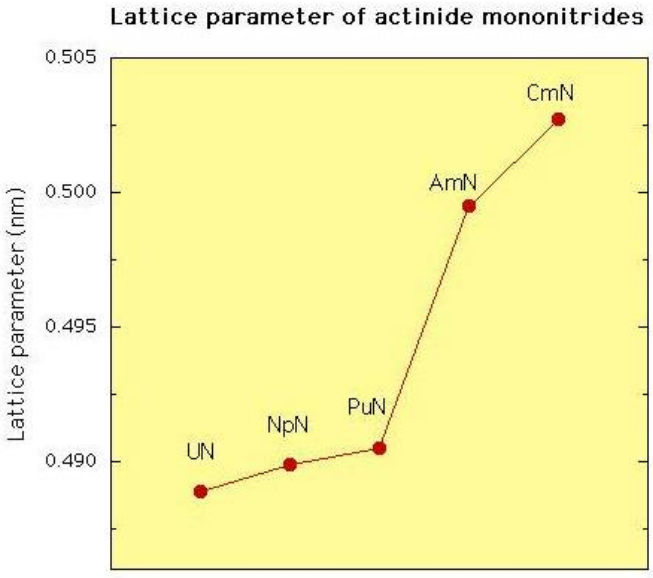

Fig. 2-2-1 Lattice parameters of UN, NpN, PuN, AmN and CmN

2.2.2 Lattice parameter and theoretical density of (U,Pu)N

Lattice parameter of $(U_{1-x}Pu_x)N$ at room temperature is calculated from the following equation assuming the Vegard's law between UN and PuN. Lattice parameters of UN and PuN are cited from the review by Benedict [16].

$$a\ (nm) = 0.48887 + 1.63\times10^{-3}\ x \qquad (2\text{-}2\text{-}1)$$

Similarly, theoretical density of $(U_{1-x}Pu_x)N$ at room temperature is calculated from the following equation, in which M_U and M_{Pu} denote the mass number of U and Pu, respectively, and 14.01 is the mass number of natural nitrogen. The uncertainty is evaluated to be less than ± 1 %.

$$D\ (g/cm^3) = 6.642\times10^{-3}\ \{(1-x)\ M_U + x\ M_{Pu} + 14.01\} / a^3 \qquad (2\text{-}2\text{-}2)$$

Fig. 2-2-2 shows the composition dependence of lattice parameter and theoretical density of $(U_{1-x}Pu_x)N$ calculated from Eq. (2-2-1) and Eq. (2-2-2), respectively, assuming M_U=238.03 and M_{Pu}=239.26.

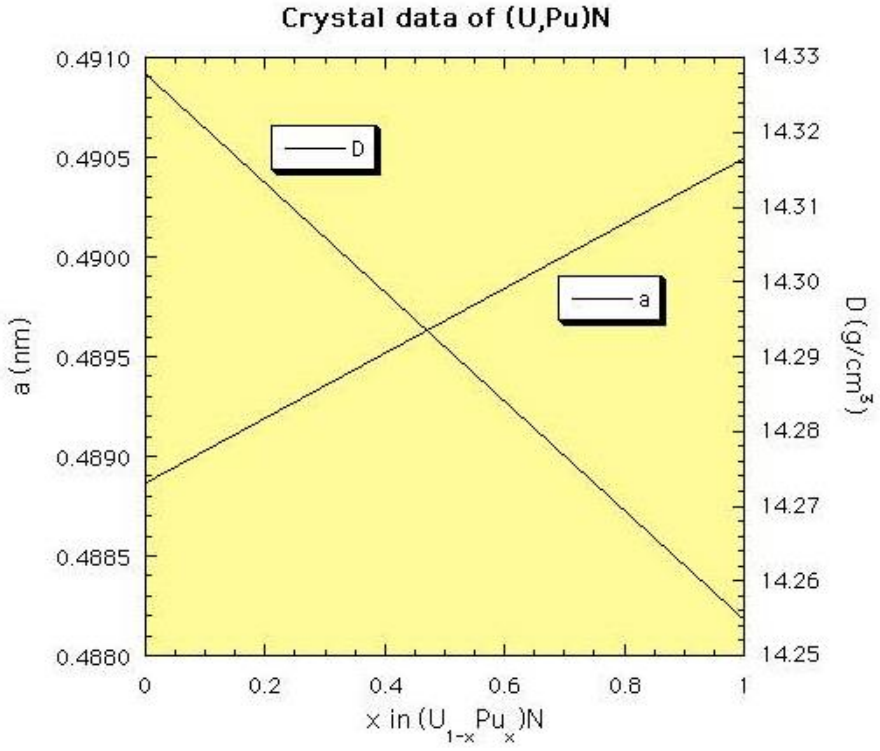

Fig. 2-2-2 Lattice parameter and theoretical density of $(U_{1-x}Pu_x)N$ with natural nitrogen

In case N-15 enriched nitrogen to 99.9% is used, theoretical density of $(U_{1-x}Pu_x)^{15}N$ is

calculated from Eq. (2-2-3).

$$D\ (g/cm^3) = 6.642\times10^{-3}\ \{(1-x)\ M_U + x\ M_{Pu} + 15.00\} / a^3 \qquad (2\text{-}2\text{-}3)$$

2.2.3 Lattice parameter and theoretical density of $(Zr_{1-w-x-y-z}Np_wPu_xAm_yCm_z)N$

Lattice parameter of $(Zr_{1-w-x-y-z}Np_wPu_xAm_yCm_z)N$ solid solution at room temperature is calculated from the following equation assuming the Vegard's law between NpN, PuN, AmN, CmN and ZrN. Lattice parameters of the respective mononitrides are cited from the paper by Takano [17]. The uncertainty is less than ± 0.001 nm.

$$a\ (nm) = 0.45756 + 3.204\times10^{-2}\ w + 3.294\times10^{-2}\ x + 4.154\times10^{-2}\ y + 4.514\times10^{-2}\ z \qquad (2\text{-}2\text{-}4)$$

Similarly, theoretical density of $(Zr_{1-w-x-y-z}Np_wPu_xAm_yCm_z)N$ solid solution at room temperature is calculated from the following equation, in which M_{Np}, M_{Pu}, M_{Am}, and M_{Cm} denote the mass number of Np, Pu, Am and Cm, respectively, and 91.22 is the mass number of Zr. The uncertainty is evaluated to be less than ± 1 %.

$$D\ (g/cm^3) = 6.642\times10^{-3}\ (105.23+w(M_{Np}-91.22)+x(M_{Pu}-91.22)+y(M_{Am}-91.22)+z(M_{Cm}-91.22))/\ a^3 \qquad (2\text{-}2\text{-}5)$$

When M_{Np}=237, M_{Pu}=239.26, M_{Am},=241, M_{Cm}=244,

$$D\ (g/cm^3) = 6.642\times10^{-3}\ (105.23 + 145.78\ w + 148.04\ x + 149.78\ y + 152.78\ z) / a^3 \qquad (2\text{-}2\text{-}6)$$

Fig. 2-2-3 shows the composition dependence of lattice parameter and theoretical density of $(Zr_{1-2x}Pu_xAm_x)N$ calculated from Eq. (2-2-4) and Eq. (2-2-6), respectively.

In case N-15 enriched nitrogen to 99.9% is used, theoretical density of $(Zr_{1-w-x-y-z}Np_wPu_xAm_yCm_z)^{15}N$ is calculated from the following equation.

$$D\ (g/cm^3) = 6.642\times10^{-3}\ (106.22 + 145.78\ w + 148.04\ x + 149.78\ y + 152.78\ z) / a^3 \qquad (2\text{-}2\text{-}7)$$

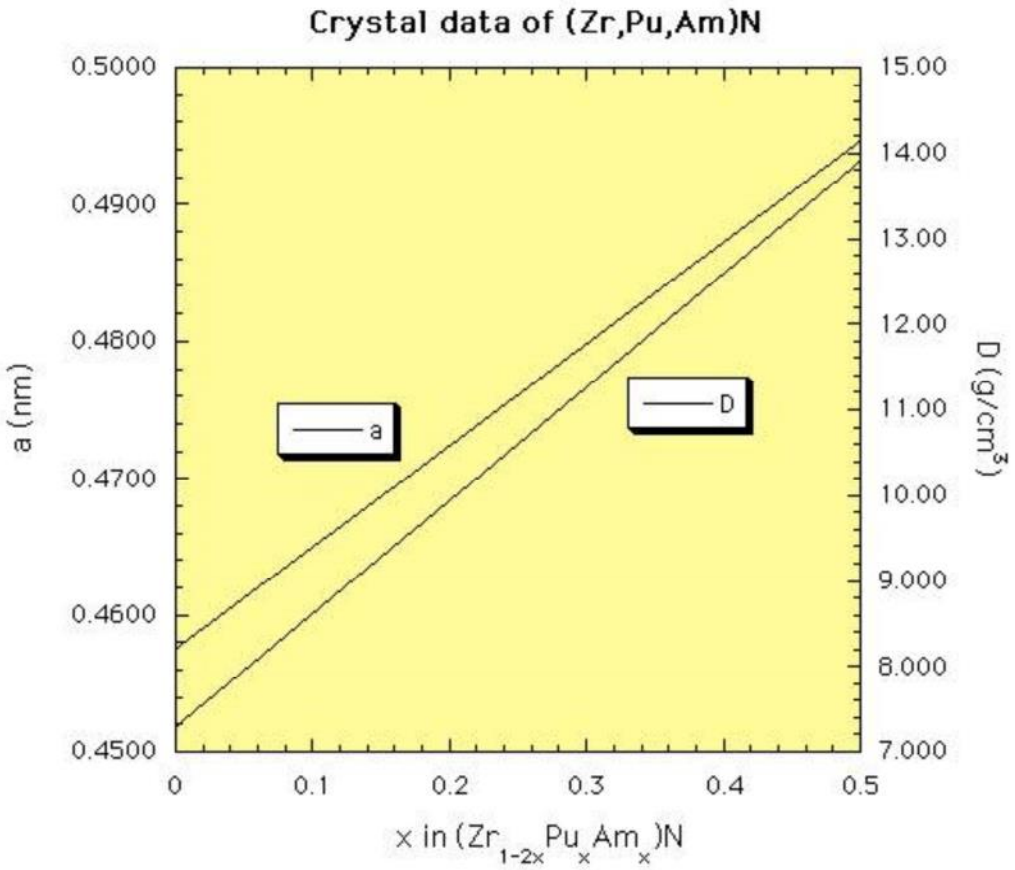

Fig. 2-2-3 Lattice parameter and theoretical density of $(Zr_{1-2x}Pu_xAm_x)N$ with natural nitrogen

2.2.4 Densities of UN, PuN and (U,Pu)N in liquid state

Sheth and Leibowitz evaluated the densities of UN, PuN and $(U_{0.8}P_{0.2})N$ in liquid state, assuming that the volume change at melting, $\Delta V/V_s$, is 15 % and the ratio of thermal expansion coefficient of solid and liquid, α_s/α_l, is 0.5 [18]. Based on these assumptions, density in liquid state is calculated from the following equation.

$$D(T) = D_{298} / [1.15 \times \{1 + 3\ (T_m\text{-}298)\ \alpha_s\} \times \{1 + 3\ (T\text{-}T_m)\ \alpha_l\}] \qquad (2\text{-}2\text{-}8)$$

Fig. 2-2-4 shows the results calculated from Eq. (2-2-8), in case of the values in Table 2-2-2 for D_{298}, T_m, α_s and α_l of UN, PuN and $(U_{0.8}P_{0.2})N$. However, there are several uncertainties in the evaluated density in liquid state. Further, as the dissociation progressing at high temperature, the density may be close to that of metallic state. The uncertainty is presumed to be about ± 10 %.

Table 2-2-2 Values used for calculating density of UN, PuN and $(U_{0.8}Pu_{0.2})N$ in liquid state from Eq. (2-2-8)

Compound	α_s (K^{-1})	α_l (K^{-1})	T_m (K)	$\Delta V/V_s$ (%)	D_{298} (g/cm^3)
UN	10.8×10^{-6}	21.6×10^{-6}	3035	15	14.32
PuN	19.5×10^{-6}	39.0×10^{-6}	2843	15	14.24
$(U_{0.8}Pu_{0.2})N$	11.4×10^{-6}	22.8×10^{-6}	3053	15	14.30

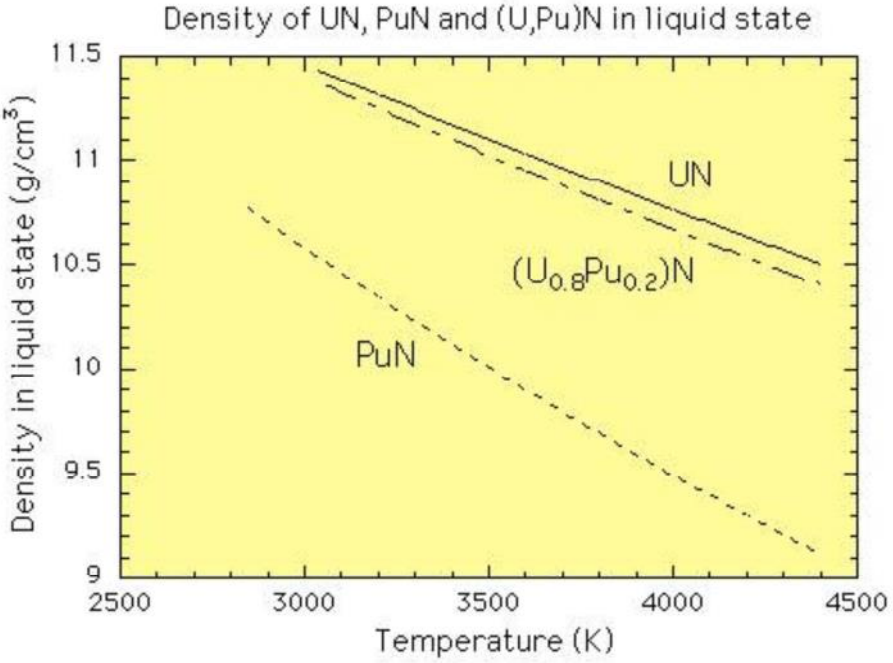

Fig. 2-2-4 Densities of UN, PuN and $(U_{0.8}Pu_{0.2})N$ in liquid state

2.2.5 Lattice expansion of PuN, AmN, CmN, (Pu,Am,Cm)N and (Np,Pu,Am,Cm)N by self-irradiation damage

Lattice expansion of PuN [19], AmN [20], CmN, (Pu,Am,Cm)N and (Np,Pu,Am,Cm)N [21] by self-irradiation damage was measured as a function of storage time at room temperature. The results are generally fitted to the following equation, in which a_t and a_0 are lattice parameter at storage time t and t=0, A and B are constants for fitting, and λ is an effective decay constant of the sample.

$$a_t = a_0 + a_0 A [1-\exp(-B\lambda t)] \qquad (2\text{-}2\text{-}9)$$

Speculated values of a_0, A, B and λ in Eq. (2-2-9) for PuN [18], AmN [19], CmN, (Pu,Am,Cm)N and (Np,Pu,Am,Cm)N [21] are shown in Table 2-2-3.

Table 2-2-3 Values of a_0, A, B and λ in Eq. (2-2-9) for PuN, AmN, CmN, (Pu,Am,Cm)N and (Np,Pu,Am,Cm)N

Compound	a_0 (nm)	A	B	λ (1/s)	Ref.
PuN	0.49054	2.54×10^{-3}	2.13×10^{4}	2.39×10^{-12}	[18]
AmN	0.4991	5.25×10^{-3}	1.96×10^{4}	5.10×10^{-11}	[19]
CmN	0.50261	4.31×10^{-3}	1.76×10^{4}	9.43×10^{-10}	[20]
$(Pu_{0.450}Am_{0.336}Cm_{0.214})N$	0.4956	4.2×10^{-3}	1.8×10^{4}	2.33×10^{-10}	[20]
$(Np_{0.279}Pu_{0.307}Am_{0.279}Cm_{0.135})N$	0.4943	4.1×10^{-3}	1.7×10^{4}	1.47×10^{-10}	[20]

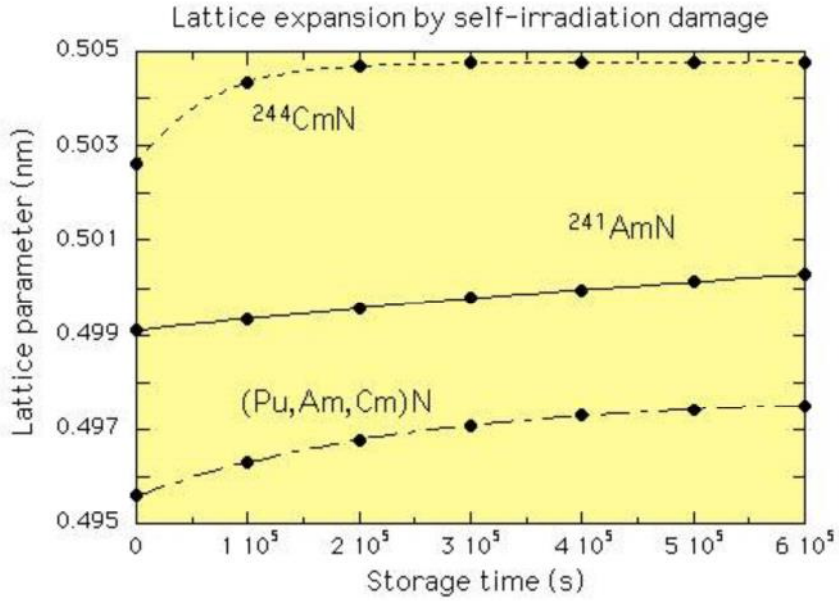

Fig. 2-2-5 Change in lattice parameters of AmN, CmN and (Pu,Am,Cm)N at room temperature as a function of storage time

Change in lattice parameter of ^{241}AmN, ^{244}CmN and $(Pu_{0.450}Am_{0.336}Cm_{0.214})N$ calculated from Eq. (2-2-9) is shown in Fig. 2-2-5.

2.3 Heat capacity

2.3.1 Heat capacities of UN, NpN, PuN, AmN and (U,Pu)N

Hayes et al. recommend the following equation for the heat capacity of UN by summarizing nine experimental data sets [9].

$$C_p(\mathrm{Jmol^{-1}K^{-1}}) = 51.14\left(\frac{365.7}{T}\right)^2 \frac{\exp\left(\frac{365.7}{T}\right)}{\left[\exp\left(\frac{365.7}{T}\right)-1\right]^2} + 9.491\times10^{-3}T + \frac{2.642\times10^{11}}{T^2}\exp\left(-\frac{18081}{T}\right)$$

$(298 < T(K) < 2628)$ (2-3-1)

The following heat capacity equation for PuN is given by Oetting [22].

$C_p\,(\mathrm{Jmol^{-1}K^{-1}}) = 1.542\times10^{-2}\,T + 45.00$ $(293 < T(K) < 1562)$ (2-3-2)

The heat capacity of NpN and AmN were determined by drop calorimetry by Nishi, et al. [23]. The heat capacity of NpN is expressed by the following equation.

$C_p\,(\mathrm{Jmol^{-1}K^{-1}}) = 1.872\times10^{-2}\,T + 42.75$ $(334 < T(K) < 1067)$ (2-3-3)

The heat capacity of AmN is expressed by the following equation.

$C_p\,(\mathrm{Jmol^{-1}K^{-1}}) = 1.563\times10^{-2}\,T + 42.44$ $(354 < T(K) < 1071)$ (2-3-5)

The following heat capacity equation for $(U_{0.8}Pu_{0.2})N$ is given by Alexander, et al. [24].

$C_p\,(\mathrm{Jmol^{-1}K^{-1}}) = 1.09\times10^{-2}\,T + 45.4$ $(293 < T(K) < 2073)$ (2-3-6)

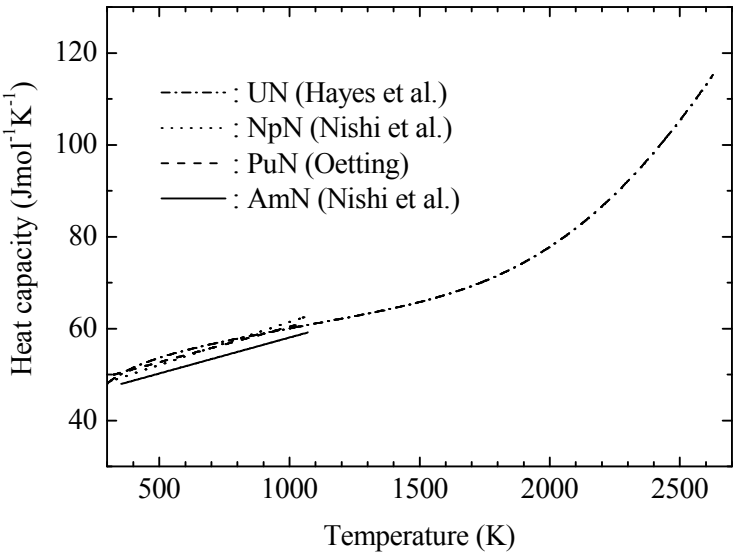

Fig. 2-3-1 Heat capacities of UN, NpN, PuN and AmN

The uncertainty of heat capacities shown in Fig. 2-3-1 is evaluated to be less than ± 10 %.

An attempt to evaluate C_p ($Jmol^{-1}K^{-1}$) for UN and $(U_{0.8}Pu_{0.2})N$ at liquid state was also made [1]. The evaluated C_p ($Jmol^{-1}K^{-1}$) are 75.8 for UN and 77.2 for $(U_{0.8}Pu_{0.2})N$ at 4000 K, while 88.7 for UN and 90.9 for $(U_{0.8}Pu_{0.2})N$ at 6000 K.

2.3.2 Heat capacity of (Zr,Pu,Am)N

The heat capacity of (Zr,Pu,Am)N is expressed as the following equation.

$$C_p\ (Jmol^{-1}K^{-1}) = a\ T + b - c\ T^{-2} \qquad (2\text{-}3\text{-}7)$$

The coefficients a, b and c in Eq. (2-3-7) for $(Zr_{0.61}Pu_{0.39})N$ [25], $(Zr_{0.58}Pu_{0.21}Am_{0.21})N$ and $(Zr_{0.80}Pu_{0.10}Am_{0.10})N$ [26] are summarized in Table 2-3-1. The uncertainty of the heat capacities shown in Fig. 2-3-2 is less than ± 5 %.

Table 2-3-1 Coefficients a, b and c in Eq. (2-3-7) for $(Zr_{0.61}Pu_{0.39})N$, $(Zr_{0.58}Pu_{0.21}Am_{0.21})N$ and $(Zr_{0.80}Pu_{0.10}Am_{0.10})N$

	$(Zr_{0.61}Pu_{0.39})N$ $298 \leq T(K) \leq 1100$	$(Zr_{0.58}Pu_{0.21}Am_{0.21})N$ $298 \leq T(K) \leq 1082$	$(Zr_{0.80}Pu_{0.10}Am_{0.10})N$ $298 \leq T(K) \leq 1067$
a	8.8807×10^{-3}	7.6556×10^{-4}	1.2836×10^{-3}
b	8.8807	56.322	42.542
c	-	1.5865×10^{6}	6.6356×10^{5}

The heat capacity of ZrN is given by the following equation in the thermodynamic database [27].

$$C_p\ (Jmol^{-1}K^{-1}) = 45.86 + 6.82\times10^{-3}\ T - 5.54\times10^{5}\ T^{-2} \qquad (2\text{-}3\text{-}8)$$

The heat capacity of $(Zr_{1-x-y-z}Np_xPu_yAm_z)N$ is given by the following equation from Eq. (2-3-2), Eq. (2-3-3), Eq. (2-3-4) and Eq. (2-3-8) assuming the Neumann-Kopp's law to the solid solution.

$$C_p\ (Jmol^{-1}K^{-1}) = 45.86 + 6.82\times10^{-3}\ T - 5.54\times10^{5}\ T^{-2} - x\ (3.11 - 1.19\times10^{-2}\ T - 5.54\times10^{5}\ T^{-2}) - y\ (0.86 - 8.60\times10^{-3}\ T - 5.54\times10^{5}\ T^{-2}) - z\ (3.42 - 8.81\times10^{-3}\ T - 5.54\times10^{5}\ T^{-2}) \qquad (2\text{-}3\text{-}9)$$

The maximum uncertainty of the heat capacity of $(Zr_{1-x-y-z}Np_xPu_yAm_z)N$ calculated from Eq. (2-3-9) is evaluated as ± 20 % at 1673 K.

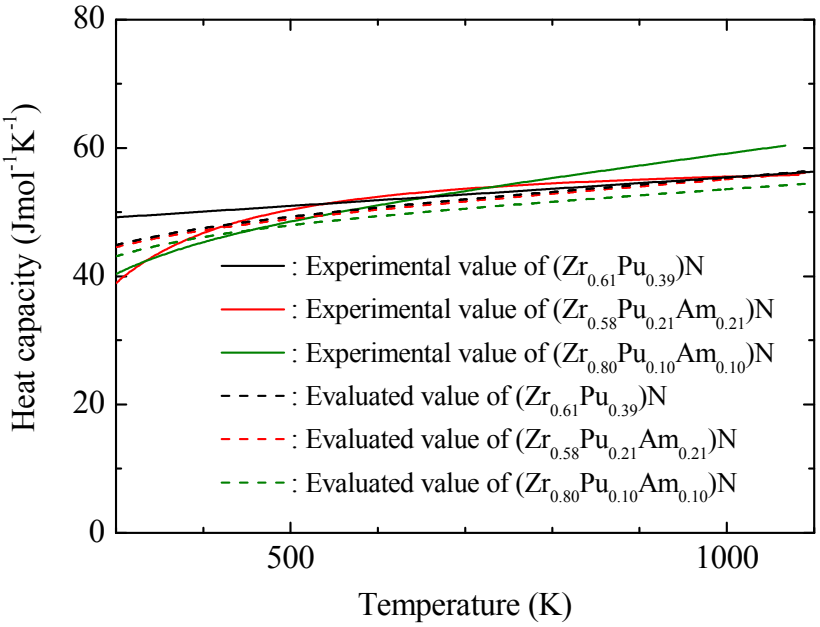

Fig. 2-3-2 Heat capacities of $(Zr_{0.61}Pu_{0.39})N$, $(Zr_{0.58}Pu_{0.21}Am_{0.21})N$ and $(Zr_{0.80}Pu_{0.10}Am_{0.10})N$

2.4 Thermal conductivity

2.4.1 Calibration of thermal conductivity to theoretical density

In this study, to compare the thermal conductivities of TRU nitrides, the data are corrected to 100%TD (TD: theoretical density) following the Schulz' equation [28].

$$K\ (Wm^{-1}K^{-1}) = K_{TD}\ (1-P)^{X} \qquad (2\text{-}4\text{-}1)$$

where K_{TD} is the thermal conductivity of the sample with 100%TD, P is the porosity of the sample, and X=1.5 is the parameter for closed pores of spherical shape. Among a variety of porosity correction formulae, the Schulz' equation is in best agreement with the result of finite element computations over a wide range of porosity up to 0.3, as reported by Bakker et al. [29]. Morimoto, et al. suggested that the analytical error is about 8 % when thermal conductivities are normalized using Schulz equation [30].

2.4.2 Thermal conductivities of UN, NpN, PuN and AmN

There are several data sets of thermal conductivities of UN and PuN. The thermal conductivities of UN, NpN and PuN were measured by Arai, et al. from 680 to 1600 K [31,32] and that of AmN was measured by Nishi, et al. from 473 to 1473 K [33]. The UN, NpN, PuN and AmN samples were prepared by the carbothermic reduction of the respective dioxides [31-33]. The thermal conductivities of actinide mononitrides increase with temperature over the temperature range investigated. The increase is due to the increase of electronic contribution to thermal conductivity.

The measured thermal conductivities of UN, NpN, PuN and AmN, K ($Wm^{-1}K^{-1}$), corrected for porosity to 100%TD are fitted to the quadratic function or cubic function (only UN) of temperature T (K) using the least squares method.

$$K\ (Wm^{-1}K^{-1}) = A + B\,T + C\,T^2 + D\,T^3 \qquad (2\text{-}4\text{-}2)$$

The coefficients A, B, C and D in Eq. (2-4-2) for UN, NpN, PuN and AmN are summarized in Table 2-4-1.

Table 2-4-1 Coefficients A, B, C and D in Eq. (2-4-2) for UN, NpN, PuN and AmN

	UN	NpN	PuN	AmN
A	-17.75	7.89	8.18	8.99
B	8.81×10^{-2}	1.27×10^{-2}	5.22×10^{-3}	1.47×10^{-3}
C	-6.16×10^{-5}	-4.32×10^{-6}	-9.44×10^{-7}	-2.54×10^{-8}
D	1.45×10^{-8}	-	-	-

The thermal conductivities calculated from Eq. (2-4-2) are shown in Fig. 2-4-1. The uncertainty of the thermal conductivities calculated from Eq. (2-4-2) is less than ± 10 %.

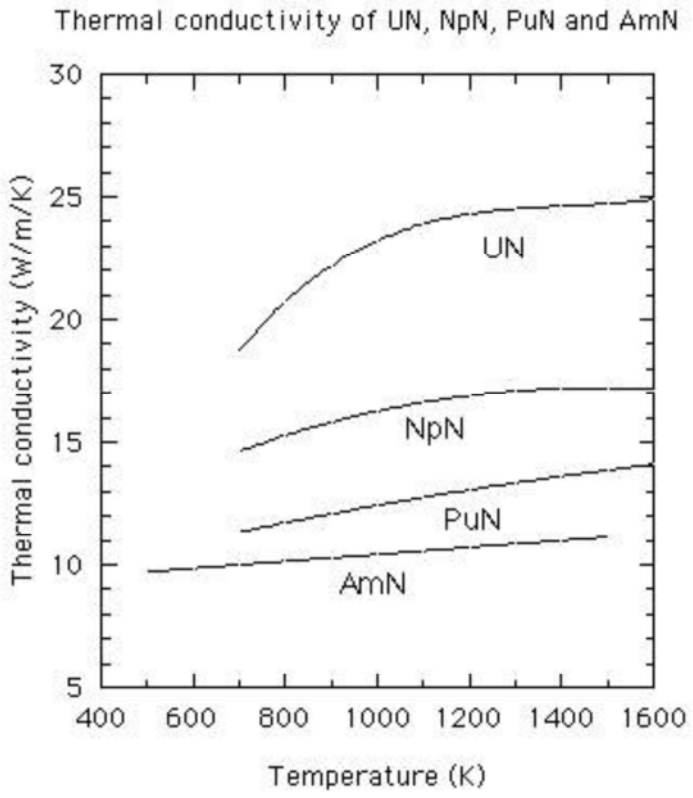

Fig. 2-4-1 Thermal conductivities of UN, NpN, PuN and AmN

Thermal conductivities of actinide mononitrides decrease with increase in the atomic number of actinide element. They increase with temperature over the temperature range investigated [15].

2.4.3 Thermal conductivity of (U,Pu)N

The pellets of (U,Pu)N solid solutions were prepared by heating green disks of mixture of UN and PuN prepared by the carbothermic reduction of the respective dioxides [31]. Measured thermal conductivity of $(U_{1-x}Pu_x)N$ (x = 0, 0.2, 0.35, 0.6, 0.8, 1), K ($Wm^{-1}K^{-1}$), corrected for porosity to 100%TD is fitted to the quadratic function or cubic function (only UN) of temperature T (K) using the least squares method [31]. The coefficients A, B, C and D in Eq. (2-4-2) for $(U_{1-x}Pu_x)N$ are summarized in Table 2-4-2.

Table 2-4-2 Coefficients A, B, C and D in Eq. (2-4-2) for $(U_{1-x}Pu_x)N$

x	0	0.2	0.35	0.6	0.8	1
A	-17.75	6.65	4.40	4.33	3.98	8.18
B	8.81×10^{-2}	1.72×10^{-2}	1.57×10^{-2}	1.29×10^{-2}	1.15×10^{-2}	5.22×10^{-3}
C	-6.16×10^{-5}	-4.68×10^{-6}	-4.03×10^{-6}	-3.46×10^{-6}	-2.90×10^{-6}	-9.44×10^{-7}
D	1.45×10^{-8}	-	-	-	-	-

Thermal diffusivity was measured by laser flash method from 680 to 1620 K. Heat capacities of UN and PuN were cited from literature, and that of $(U_{1-x}Pu_x)N$ was estimated assuming the Neumann-Kopp's law. The thermal conductivity calculated from Eq. (2-4-2) is shown in Fig. 2-4-2 from 700 to 1600 K. The thermal conductivity decreased with x in $(U_{1-x}Pu_x)N$.

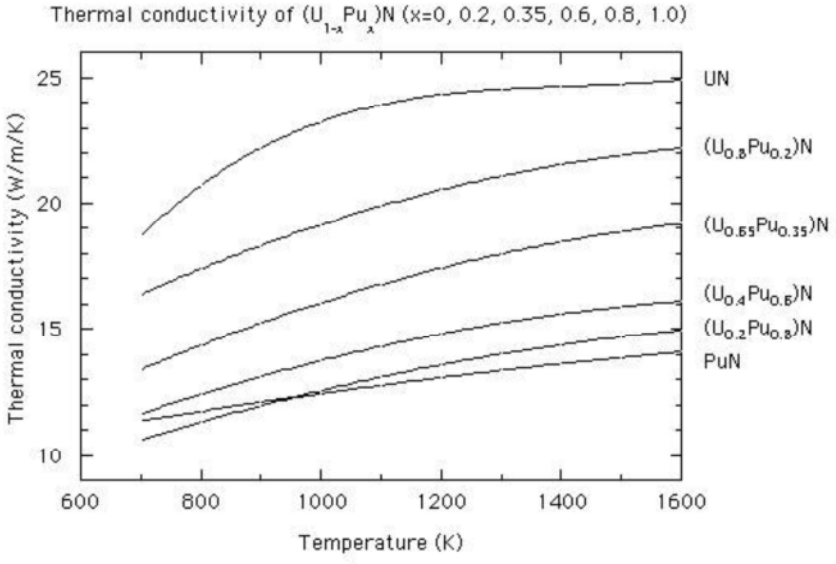

Fig. 2-4-2 Thermal conductivity of (U,Pu)N

On the other hand, the thermal conductivity of $(U_{1-x}Pu_x)N$ $(0.0 \leq x \leq 1.0)$ corrected for porosity to 100%TD is formulated by Eq. (2-4-3) as a function of temperature and composition,

$$K\ (Wm^{-1}K^{-1}) = E + F\,x + G\,x^2, \qquad (2\text{-}4\text{-}3)$$

$$E = -13.23 + 0.07706\,T - 0.00005291\,T^2 + 0.00000001234\,T^3$$
$$F = 64.58 - 0.2235\,T - 0.0001812\,T^2 - 0.00000004654\,T^3$$
$$G = -46.97 + 0.1611\,T - 0.0001367\,T^2 + 0.00000003605\,T^3$$

where E, F and G are coefficients obtained by the least-square fitting. The temperature dependences of the coefficients of E, F and G, obtained at each temperature above 700 K, are given as a polynomial equation of temperature. The uncertainty of the thermal conductivities obtained by the above equation is estimated as ± 5%, from analytical and experimental errors. The thermal conductivities of (U,Pu)N predicted from Eq. (2-4-3) are shown in Fig. 2-4-3.

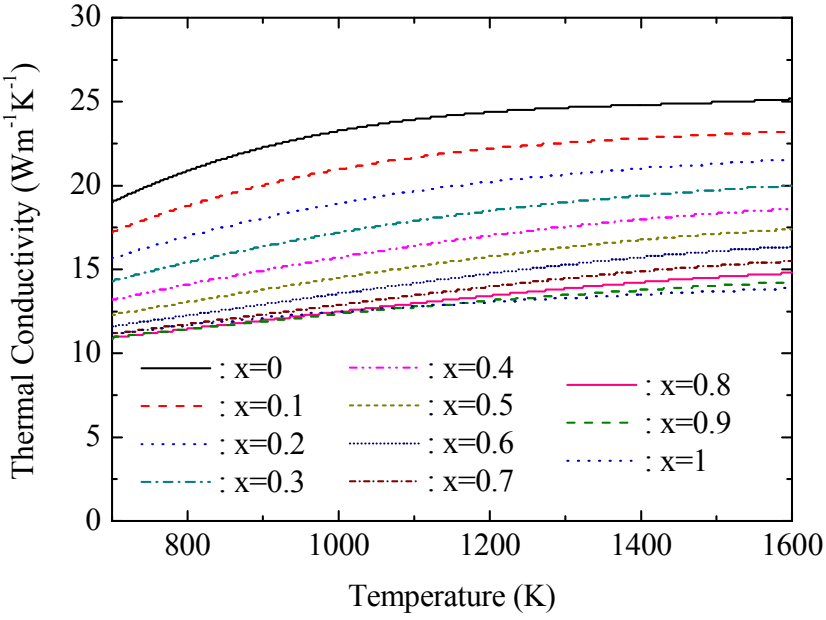

Fig. 2-4-3 Predicted thermal conductivity of $(U_{1-x}Pu_x)N$

2.4.4 Thermal conductivities of (Zr,Pu)N and (Zr,Pu,Am)N

The (Zr,Pu)N [25,34,35] and (Zr,Pu,Am)N [26] samples were prepared as follows. The ZrN powder is fabricated from highly pure Zr metal after hydrogenation and pulverization. The PuN and AmN are fabricated via the carbothermic reduction of the respective dioxides. The mixture is gradually heated to 1793 K in the purified N_2 or N_2+4%H_2 gas flow. The resultant powder was pressed into disks and sintered in a stream of N_2 or N_2+4%H_2 at

1923-1973 K to prepare (Zr,Pu)N and (Zr,Pu,Am)N pellets. The thermal conductivities of (Zr,Pu)N [25,34,35] and (Zr,Pu,Am)N [26] reported are shown in Fig. 2-4-4. The large difference of thermal conductivities of (Zr,Pu)N between the results was thought to be derived from the difference in characteristics of ZrN used in the experiments. It was seen that the oxygen impurity effect (0.34 wt.% vs. 0.65 wt.%) in (Zr,Pu)N is very limited [25].

Measured thermal conductivities of $(Zr_{0.61}Pu_{0.39})N$, $(Zr_{0.61}Pu_{0.39})(N,O)$ [25], $(Zr_{0.58}Pu_{0.21}Am_{0.21})N$ and $(Zr_{0.80}Pu_{0.10}Am_{0.10})N$ [26], K ($Wm^{-1}K^{-1}$), corrected for porosity to 100%TD are fitted to the quadratic function ((Zr,Pu,Am)N) or cubic function ((Zr,Pu)N) of temperature T (K) using the least squares method. The coefficients A, B, C and D in Eq. (2-4-2) for (Zr,Pu)N and (Zr,Pu,Am)N are summarized in Table 2-4-3.

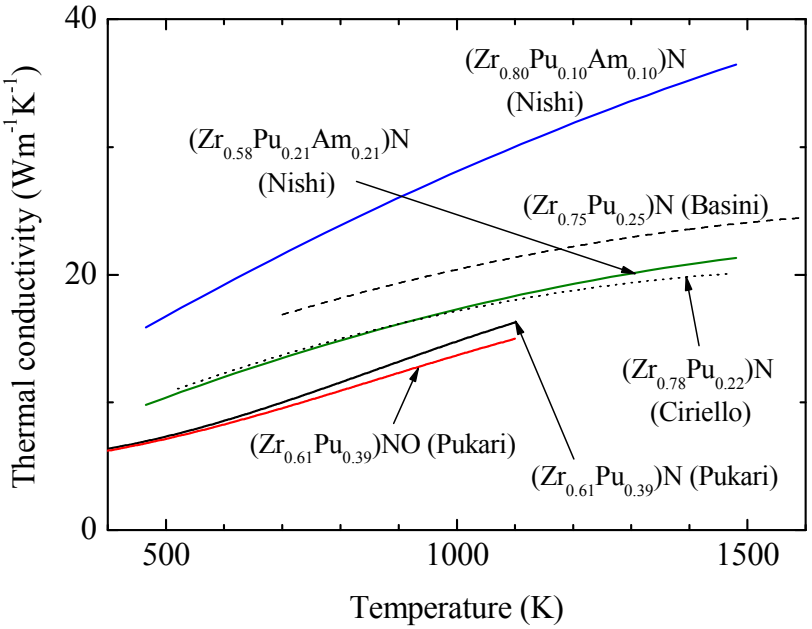

Fig. 2-4-4 Thermal conductivities of (Zr,Pu)N and (Zr,Pu,Am)N

Table 2-4-3 Coefficients A, B, C and D in Eq. (2-4-2) for (Zr,Pu)N and (Zr,Pu,Am)N

	$(Zr_{0.61}Pu_{0.39})N$ $298 \leq T(K) \leq 1100$	$(Zr_{0.61}Pu_{0.39})(N,O)$ $298 \leq T(K) \leq 1100$	$(Zr_{0.58}Pu_{0.21}Am_{0.21})N$ $473 \leq T(K) \leq 1473$	$(Zr_{0.80}Pu_{0.10}Am_{0.10})N$ $473 \leq T(K) \leq 1473$
A	6.958	5.633	0.716	2.73
B	-1.285×10^{-2}	-6.654×10^{-3}	2.21×10^{-2}	3.07×10^{-2}
C	3.364×10^{-5}	2.399×10^{-5}	-5.52×10^{-6}	-5.34×10^{-6}
D	-1.298×10^{-8}	-9.291×10^{-9}	-	-

The thermal conductivity of $(Zr_xPu_{(1-x)/2}Am_{(1-x)/2})N$ $(0.0 \leq x \leq 1.0)$ corrected for porosity to

100%TD is formulated by the following equation using the least squares method [26].

$$K\ (Wm^{-1}K^{-1}) = A + B\exp(x/C) \qquad (2\text{-}4\text{-}4)$$

$$A = 4.7624 + 1.3937\times10^{-2}\,T - 1.4543\times10^{-5}\,T^2 + 5.6365\times10^{-9}\,T^3$$
$$B = -0.15962 - 4.2325\times10^{-4}\,T + 9.1965\times10^{-7}\,T^2$$
$$C = -9.8103\times10^{-3} + 2.3662\times10^{-4}\,T - 3.2471\times10^{-8}\,T^2$$

where x is the molar fraction of ZrN, and A, B and C are coefficients obtained by fitting. The temperature dependencies of the coefficients of A, B and C, obtained at each temperature above 873 K, are given as a polynomial equation of temperature. The predicted thermal conductivity of (Zr,Pu,Am)N is shown in Fig. 2-4-5. The uncertainty of the thermal conductivities obtained by above equation is estimated as ± 15 %, from analytical and experimental errors.

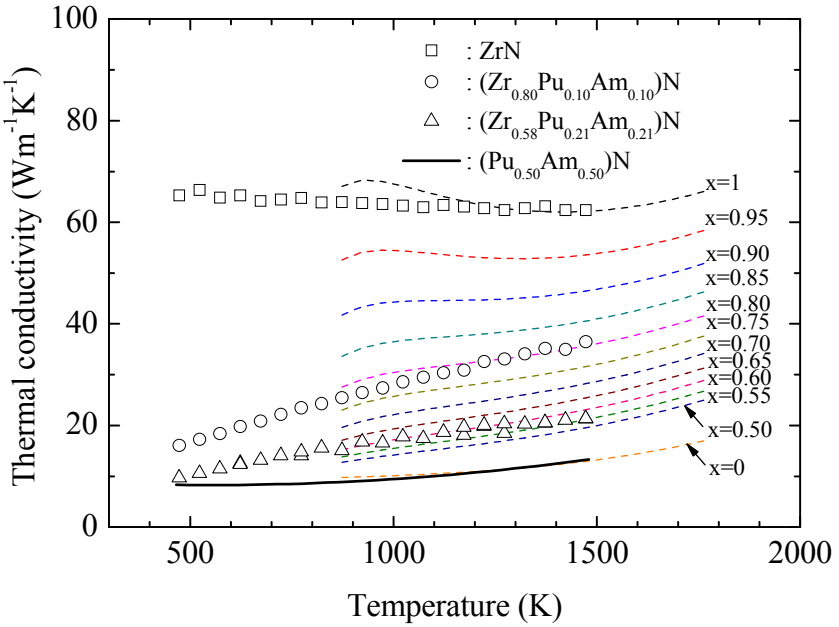

Fig. 2-4-5 Predicted thermal conductivity of $(Zr_xPu_{(1-x)/2}Am_{(1-x)/2})N$

2.4.5 Thermal conductivities of (U,Np)N and (Np,Pu)N

The pellets of (U,Np)N and (Np,Pu)N solid solutions were prepared by heating green disks of mixture of respective mononitrides. The actinide mononitride samples were prepared by the carbothermic reduction of the respective dioxides [36]. Measured thermal conductivity of $(U_{1-x}Np_x)N$ (x = 0, 0.25, 0.5, 0.75, 1), K ($Wm^{-1}K^{-1}$), corrected for porosity to 100%TD is fitted to the quadratic function or cubic function (only UN) of temperature T (K) using the least squares method [36]. The coefficients A, B, C and D in Eq. (2-4-2) for $(U_{1-x}Np_x)N$ are summarized in Table 2-4-4.

Table 2-4-4 Coefficients A, B, C and D in Eq. (2-4-2) for $(U_{1-x}Np_x)N$

x	0	0.25	0.5	0.75	1
A	-17.75	3.75	10.85	7.43	7.89
B	8.81×10^{-2}	2.14×10^{-2}	7.46×10^{-3}	1.29×10^{-2}	1.27×10^{-2}
C	-6.16×10^{-5}	-5.69×10^{-6}	-4.03×10^{-7}	-3.56×10^{-6}	-4.32×10^{-6}
D	1.45×10^{-8}	-	-	-	-

Thermal diffusivity was measured by laser flash method from 680 to 1620 K. Heat capacities of UN and NpN were cited from literature, and that of $(U_{1-x}Np_x)N$ was estimated assuming the Neumann-Kopp's law. The thermal conductivity calculated from Eq. (2-4-2) is shown in Fig. 2-4-6 from 700 to 1600 K.

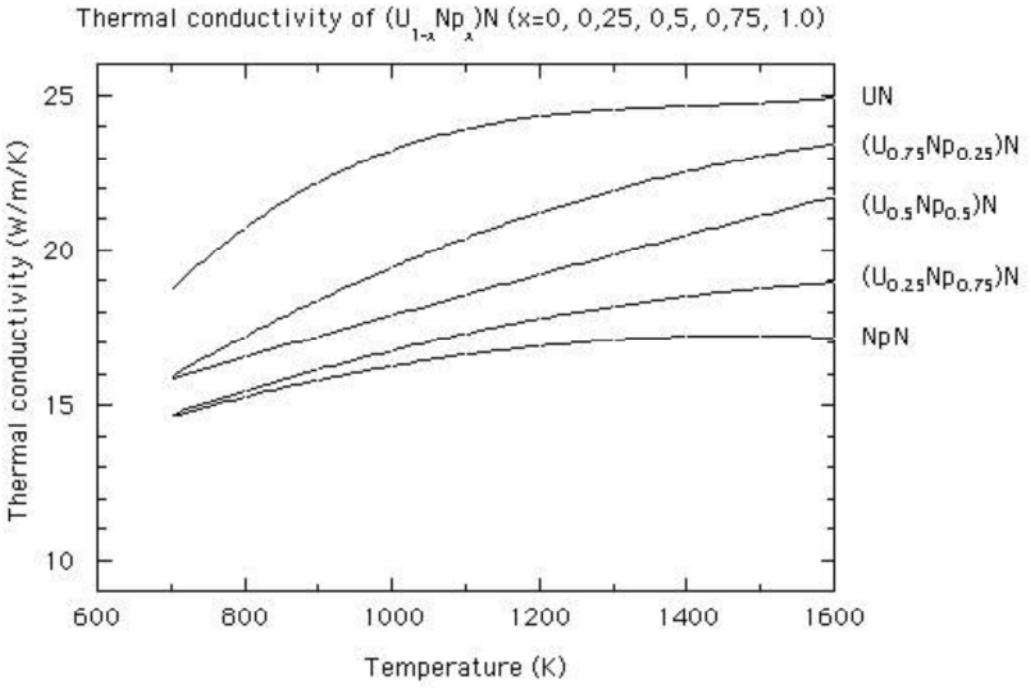

Fig. 2-4-6 Thermal conductivity of $(U_{1-x}Np_x)N$

Measured thermal conductivity of $(Np_{1-x}Pu_x)N$ (x = 0, 0.33, 0.67, 1), K ($Wm^{-1}K^{-1}$), corrected for porosity to 100%TD is fitted to the quadratic function of temperature T (K) using the least squares method [36]. The coefficients A, B and C in Eq. (2-4-2) for $(Np_{1-x}Pu_x)N$ are summarized in Table 2-4-5.

Table 2-4-5 Coefficients A, B, and C in Eq. (2-4-2) for $(Np_{1-x}Pu_x)N$

x	0	0.33	0.67	1
A	7.89	7.22	10.19	8.18
B	1.27×10^{-2}	6.91×10^{-3}	1.36×10^{-3}	5.22×10^{-3}
C	-4.32×10^{-6}	-1.28×10^{-6}	4.58×10^{-7}	-9.44×10^{-7}

Thermal diffusivity was measured by laser flash method from 680 to 1620 K. Heat capacities of NpN and PuN were cited from literature, and that of $(Np_{1-x}Pu_x)N$ was estimated assuming the Neumann-Kopp's law. The thermal conductivity calculated from Eq. (2-4-2) is shown in Fig. 2-4-7 from 700 to 1600 K.

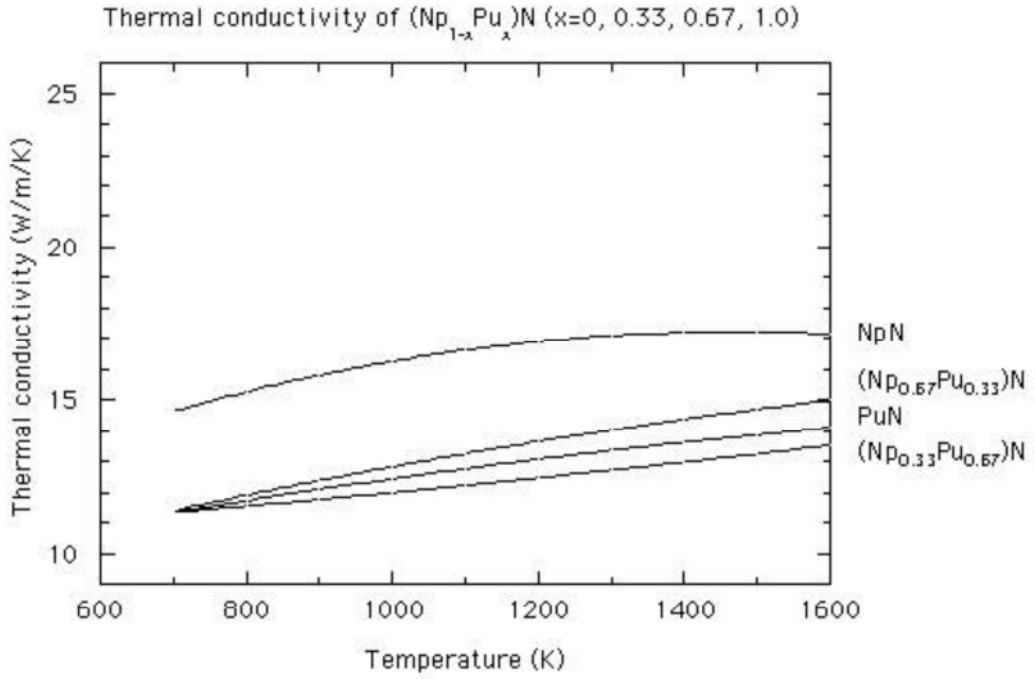

Fig. 2-4-7 Thermal conductivity of $(Np_{1-x}Pu_x)N$

2.4.6 Thermal conductivities of (Np,Am)N and (Pu,Am)N

Thermal conductivities of $(Np_{1-x}Am_x)N$ and $(Pu_{1-x}Am_x)N$ were measured by Nishi et al. from 473 to 1073 K [37]. The $(Np_{1-x}Am_x)N$ and $(Pu_{1-x}Am_x)N$ solid solution samples were prepared by the carbothermic reduction of the dioxide mixtures. Measured thermal conductivities of $(Np_{1-x}Am_x)N$ (x = 0.25, 0.50, 0.75) and $(Pu_{1-x}Am_x)N$ (x = 0.25, 0.50), K ($Wm^{-1}K^{-1}$), corrected for porosity to 100%TD are fitted to the quadratic function of temperature T (K) using the least squares method.

The experimental results shown in Fig. 2-4-8 suggest that the thermal conductivities of $(Np_{1-x}Am_x)N$ and$(Pu_{1-x}Am_x)N$ decrease with increasing Am content. The coefficients A, B and C in Eq. (2-4-2) for $(Np_{1-x}Am_x)N$ and$(Pu_{1-x}Am_x)N$ are summarized in Table 2-4-6.

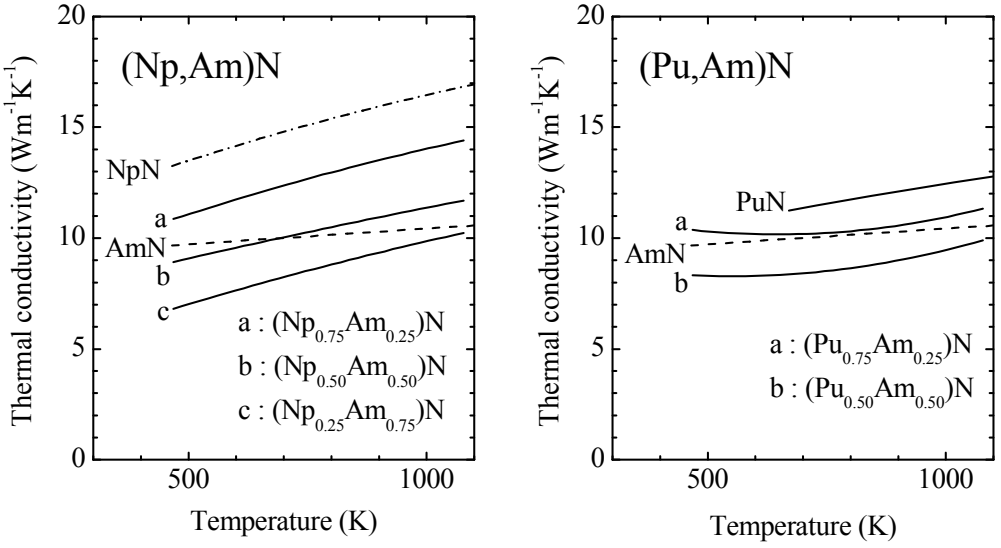

Fig. 2-4-8 Thermal conductivities of $(Np_{1-x}Am_x)N$ and$(Pu_{1-x}Am_x)N$

Table 2-4-6 Coefficients A, B, and C in Eq. (2-4-2) for $(Np_{1-x}Am_x)N$ and$(Pu_{1-x}Am_x)N$

	$(Np_{1-x}Am_x)N$			$(Pu_{1-x}Am_x)N$	
x	0.25	0.50	0.75	0.25	0.50
A	7.18	6.49	3.45	12.81	10.03
B	8.75×10^{-3}	5.49×10^{-3}	7.88×10^{-3}	8.16×10^{-3}	-6.39×10^{-3}
C	-1.90×10^{-6}	-6.07×10^{-7}	-1.47×10^{-6}	6.29×10^{-6}	5.82×10^{-6}

2.4.7 Thermal conductivity of (Np,Pu,Am,Cm)N

Thermal conductivity of $(Np_{0.20}Pu_{0.50}Am_{0.25}Cm_{0.05})N$ was measured by Nishi, et al. [38]. The solid solution sample was prepared by the carbothermic reduction of the dioxide mixtures. The measured thermal conductivity, K ($Wm^{-1}K^{-1}$), corrected for porosity to 100%TD is fitted to the following quadratic function of temperature T (K) using the least squares method.

$$K\ (Wm^{-1}K^{-1}) = 6.34 + 2.67\times10^{-3}\ T + 9.02\times10^{-7}\ T^2 \qquad (2\text{-}4\text{-}5)$$

Thermal diffusivity was measured by laser flash method from 293 to 1473 K. Heat capacity was estimated from those of NpN, PuN and AmN assuming the Neumann-Kopp's law, in which the heat capacity of CmN was substituted by that of AmN due to lack of the data for CmN. Fig. 2-4-9 shows the thermal conductivity of $(Np_{0.20}Pu_{0.50}Am_{0.25}Cm_{0.05})N$ calculated from Eq. (2-4-5) and experimental data as well as those of NpN, PuN and AmN.

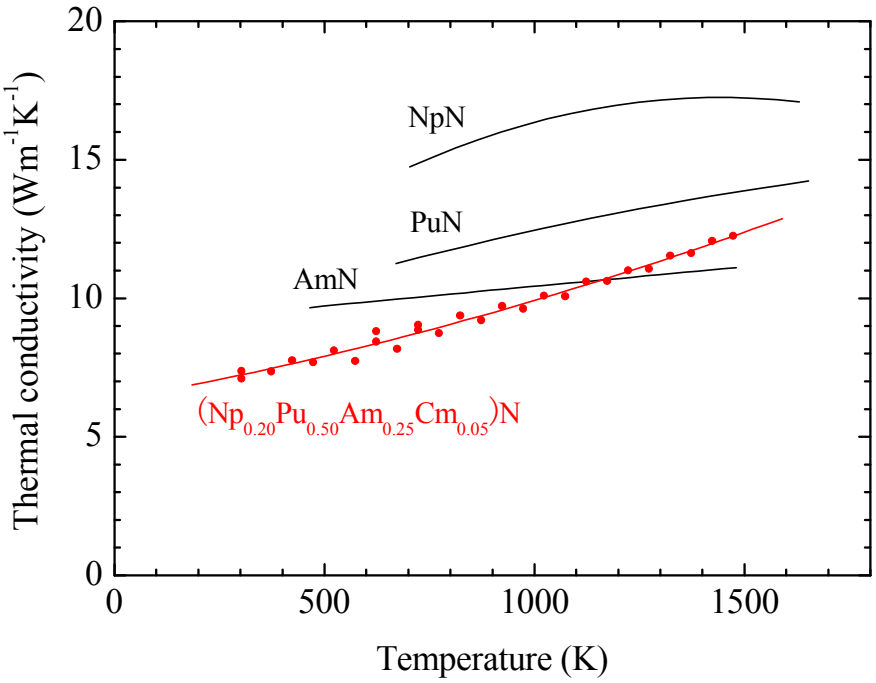

Fig. 2-4-9 Thermal conductivity of $(Np_{0.20}Pu_{0.50}Am_{0.25}Cm_{0.05})N$

2.5 Thermal expansion

2.5.1 Thermal expansions of UN, PuN, NpN, AmN and CmN

Thermal expansions of actinide mononitrides have been mostly investigated high-temperature X-ray diffractometry (HT-XRD). Regression data on temperature dependence of lattice parameters, a_T (nm), are listed in Table 2-5-1. On the other hand, regression data on linear thermal expansion, LTE (%), defined by $((a_T-a_{293})/a_{293}) \times 100$, and averaged thermal expansion coefficients over 293-1273 K, $\alpha_{av.1273}$, ($\alpha_{av.T} = (1/a_{293})(a_T-a_{293})/(T-293)$), are listed in Table 2-5-2. The data on UN are cited from the review by Hayes, et al. [6] and those on the others are cited from experimental results by Takano, et al. [21,39]. The uncertainty of the lattice parameter, LTE and thermal expansion coefficient is less than ± 3 %.

Table 2-5-1 Regression data for a_T (nm) = $a_0 + a_1 T + a_2 T^2 + a_3 T^3$

	a_0	$a_1\times10^6$	$a_2\times10^{10}$	$a_3\times10^{14}$	a_{293} (nm)	Max. Temp. (K)
UN	0.48790	3.264	6.889	-	0.48892	2523
NpN	0.48848	3.483	6.274	-7.601	0.48956	1348
PuN	0.48913	4.501	6.817	-4.939	0.49050	1478
AmN	0.49786	4.110	9.936	-3.169	0.49915	1464
CmN	0.50133	4.1361	5.9909	-6.3043	0.50261	1375

Table 2-5-2 Regression data for LTE (%) = $b_1 (T-293) + b_2 (T-293)^2 + b_3 (T-293)^3$ and $\alpha_{av.1273}$

	$b_1 \times 10^4$	$b_2 \times 10^7$	$b_3 \times 10^{12}$	LTE_{1273} (%)	$\alpha_{av.1273}$ (10^{-6}/K)
UN	7.505	1.407	-	0.87	8.88
NpN	7.827	1.142	-15.34	0.86	8.80
PuN	9.973	1.288	-9.445	1.09	11.1
AmN	9.387	1.928	-6.052	1.10	11.2
CmN	8.905	1.069	-11.95	0.96	9.84

2.5.2 Averaged thermal expansion coefficient of $(Zr_{1-w-x-y-z}Np_wPu_xAm_yCm_z)N$

It is found that the averaged thermal expansion coefficients of actinide mononitrides and ZrN solid solutions can be approximated by the linear mixture rule within the error of a few percent [40]. Based on this assumption, that of $(Zr_{1-w-x-y-z}Np_wPu_xAm_yCm_z)N$ over the temperature range of 293-1273 K, $\alpha_{av.1273}$, is calculated from the following equation. The respective averaged thermal expansion coefficients of NpN, PuN, AmN, CmN and ZrN in the same temperature range are cited from the paper by Takano, et al. [21,39]. The uncertainty of the thermal expansion coefficient is evaluated to be less than ± 5 %. Averaged thermal expansion coefficient of $(Zr_{1-2x}Pu_xAm_x)N$ calculated from Eq. (2-5-1) is shown in Fig. 2-5-1.

$$\begin{aligned}\alpha_{av.1273} &= (1-w-x-y-z)\,\alpha_{av\ ZrN} + w\,\alpha_{av\ NpN} + x\,\alpha_{av\ PuN} + y\,\alpha_{av\ AmN} + z\,\alpha_{av\ CmN} \\ &= \{7.57\,(1-w-x-y-z) + 8.80\,w + 11.1\,x + 11.2\,y + 9.80\,z\}\times 10^{-6} \\ &= 7.57\times 10^{-6} + 1.23\,w\times 10^{-6} + 3.53\,x\times 10^{-6} + 3.63\,y\times 10^{-6} + 2.23\,z\times 10^{-6} \qquad (2\text{-}5\text{-}1)\end{aligned}$$

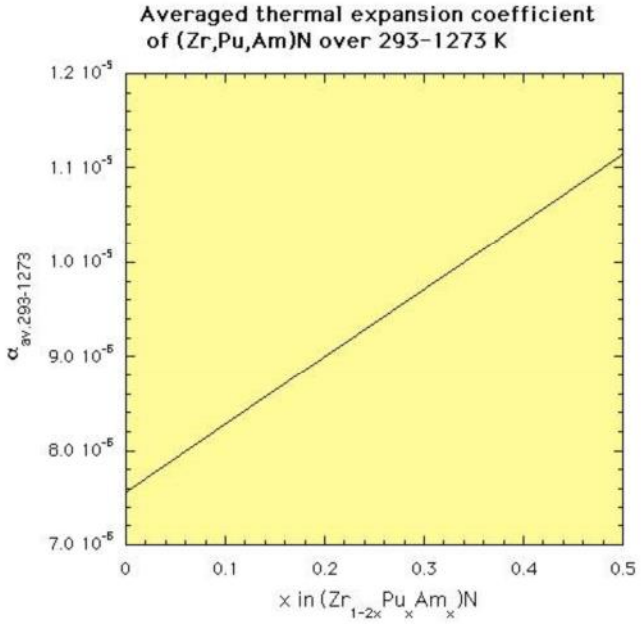

Fig. 2-5-1 Averaged thermal expansion coefficient of $(Zr_{1-2x}Pu_xAm_x)N$ over 293-1273 K

2.6 Electrical resistivity and magnetic properties

2.6.1 Electrical resistivities of UN, PuN, (U,Pu)N and (Pu,Zr)N

Matzke summarizes the electrical resistivity of UN [1]. UN is a type-I anti-ferromagnetic compound with a paramagnetic Neel temperature, T_N, of 53.1 K. At T_N, observed small peak of about 0.6 μΩcm is explained by the formation of new Brillouin-zone boundaries upon anti-ferromagnetic ordering. Above 400 K, the electrical resistivity of UN increases approximately linearly with temperature, which reflects its metallic nature. The electrical resistivity, ρ, of UN is divided into three components, contributions of magnetic spins ρ_m, phonons ρ_{ph} and temperature-independent impurities ρ_i. Hayes, et al. summarize the experimental data of UN and suggested the following fitting equation as a function of temperature ($298 \leq T(K) \leq 1600$) and porosity ($0 \leq P \leq 0.16$) [8].

$$\rho\ (\mu\Omega cm) = 71.49\ e^{2.14P}\ (T)^{0.125} \qquad (2\text{-}6\text{-}1)$$

Very limited information is available for Pu-containing nitrides. A result for PuN with low density (76%TD) indicates a pronounced increase in ρ from ~10 μΩcm below 10 K to ~650 μΩcm (~450 μΩcm, if corrected for porosity) at room temperature [41]. A result for PuN with high density indicates 450 μΩcm at 773 K and 500 μΩcm at 1173 K, being corrected for porosity to 100%TD [42].

Keller [42] also reports ρ of $(U_{0.8}Pu_{0.2})N$ that is very little dependent of temperature and fall into the range 290 to 340 μΩcm between room temperature and 1173 K. The results show that Pu addition to UN increases ρ.

Recently ρ of $(Pu_{0.39}Zr_{0.61})N$ at room temperature was measured by Pukari, et al. using a four point probe method [25]. The results suggest that ρ of $(Pu_{0.39}Zr_{0.61})N$ is close to PuN in its magnitude despite the relatively high ZrN fraction.

2.6.2 Magnetic properties of UN, NpN, PuN and AmN

Magnetic properties of UN, NpN and PuN are summarized in Table 2-6-1 [43].

Table 2-6-1 Magnetic properties of UN, NpN and PuN

	Magnetic order	T_t (K)	μ_o (μB)	μ_p (μB)	θ (K)
UN	anti-ferromagnetic	53	0.75	2.7; 3.11	-247; -325
NpN	ferromagnetic	87	1.4	2.44	100
PuN	anti-ferromagnetic	13	<0.2	1.1	-200

In Table 2-6-1, T_t, μ_o, μ_p, θ are the magnetic phase transition temperature, saturation moment per actinide ion, paramagnetic moment per actinide ion, paramagnetic Curie

(Néel) temperature, respectively. On the other hand, it is known that AmN represents temperature independent paramagnetism (TIP).

2.7 Melting temperature and decomposition pressure

2.7.1 Melting temperatures and decomposition pressures of UN, NpN, PuN and AmN

Temperature of congruent melting is reported for UN and NpN under a pressurized nitrogen atmosphere by Olson and Mulford [44,45] as summarized in Table 2-7-1. According to the same authors, however, congruent melting for PuN was not achieved in the nitrogen pressure up to 24.5 atm [46]. On the other hand, Spear and Leitnaker reported congruent melting for PuN at a still higher nitrogen pressure [47]. Hayes, et al. summarized the experimental data of melting temperature of UN and suggested the following fitting equation as a function of nitrogen partial pressure P_{N2} (atm) [9].

$$T_m\ (K) = 3035.0\ (P_{N2})^{0.02832} \quad (1\times10^{-13} \le P_{N2} \le 7.5\ atm) \tag{2-7-1}$$

On the other hand, decomposition pressures of UN, NpN and PuN following Eq. (2-7-2) are determined as a function of reciprocal temperature above 2500 K by Olson and Mulford [44-46] and fitted to Eqs. (2-7-3), (2-7-4) and (2-7-5) for UN, NpN and PuN, respectively.

$$MN(s) = M(l, \text{saturated with N}) + 0.5N_2(g) \tag{2-7-2}$$

$$\log p_{UN}(atm) = 8.193 - 29540/T + 5.57\times10^{-18}T^5 \quad (2773 \le T(K) \le 3123) \tag{2-7-3}$$

$$\log p_{NpN}(atm) = 8.193 - 29540/T + 7.87\times10^{-18}T^5 \quad (2483 \le T(K) \le 3103) \tag{2-7-4}$$

$$\log p_{PuN}(atm) = 8.193 - 29540/T + 11.28\times10^{-18}T^5 \quad (2563 \le T(K) \le 3043) \tag{2-7-5}$$

Table 2-7-1 shows the decomposition temperatures of UN, NpN and PuN under 1atm of nitrogen calculated from above equations as well as that of AmN speculated from the thermal expansion data by Takano, et al. [39]. The uncertainty of congruent melting temperature and decomposition temperature for UN, NpN and PuN is evaluated about ± 50 K.

Table 2-7-1 Summary of congruent melting temperature and decomposition temperature of actinide mononitrides under 1 atm of nitrogen

	Congruent melting temperature (K)	Decomposition temperature under 1 atom of nitrogen (K)	Reference
UN	3123 (N_2 pressure ≥ 2.5 atm)	3050	[44]
NpN	3103 (N_2 pressure ≥ 10 atm)	2960	[45]
PuN	3103±50 (N_2 pressure ≥ 50±20 atm)	2860	[46] [47]
AmN	-	~2700	[39]

2.8 Vapor pressure

2.8.1 Vapor pressures of U(g), Np(g), Pu(g) and Am(g) over UN, NpN, PuN and AmN

The major vapor species over actinide mononitrides are mono-atomic actinide gas, such as U(g), Np(g), Pu(g) and Am(g), and nitrogen gas, N_2(g).

Equilibrium vapor pressures of mono-atomic actinide gas, $p_{U(g)}$, $p_{Np(g)}$, $p_{Pu(g)}$ and $p_{Am(g)}$ over UN(s) [48], NpN(s) [49], PuN(s) [48] and AmN(s) [50] prepared by the carbothermic reduction are fitted to the following equations.

$$\log p_{U(g)}(\mathrm{Pa}) = 10.65 - 25600/T \quad (1753 \leq T(\mathrm{K}) \leq 2028) \qquad (2\text{-}8\text{-}1)$$

$$\log p_{Np(g)}(\mathrm{Pa}) = 10.26 - 22200/T \quad (1690 \leq T(\mathrm{K}) \leq 2030) \qquad (2\text{-}8\text{-}2)$$

$$\log p_{Pu(g)}(\mathrm{Pa}) = 11.74 - 22500/T \quad (1558 \leq T(\mathrm{K}) \leq 1738) \qquad (2\text{-}8\text{-}3)$$

$$\log p_{Am(g)}(\mathrm{Pa}) = 12.91 - 20200/T \quad (1623 \leq T(\mathrm{K}) \leq 1733) \qquad (2\text{-}8\text{-}4)$$

Vapor pressures of $p_{U(g)}$, $p_{Np(g)}$ and $p_{Pu(g)}$ over UN(s), NpN(s) and PuN(s) were measured by high-temperature mass spectrometry [48,49]. On the other hand, that of $p_{Am(g)}$ over AmN(s) was estimated from the Gibbs free energy of formation available in literature [51].

Vapor pressures of $p_{Pu(g)}$ and $p_{Am(g)}$ over PuN(s) and AmN (s) shown in Fig. 2-8-1 represent the congruent vaporization following PuN(s) = Pu(g) + 0.5N_2(g) and AmN(s) = Am(g) + 0.5N_2(g), respectively. On the other hand, those of $p_{U(g)}$ and $p_{Np(g)}$ over UN(s) and NpN (s) shown in the same figure represent the incongruent vaporization following UN(s) = U(l) + 0.5N_2(g), U(l) = U(g) and NpN(s) = Np(l) + 0.5N_2(g), Np(l) = Np(g), respectively.

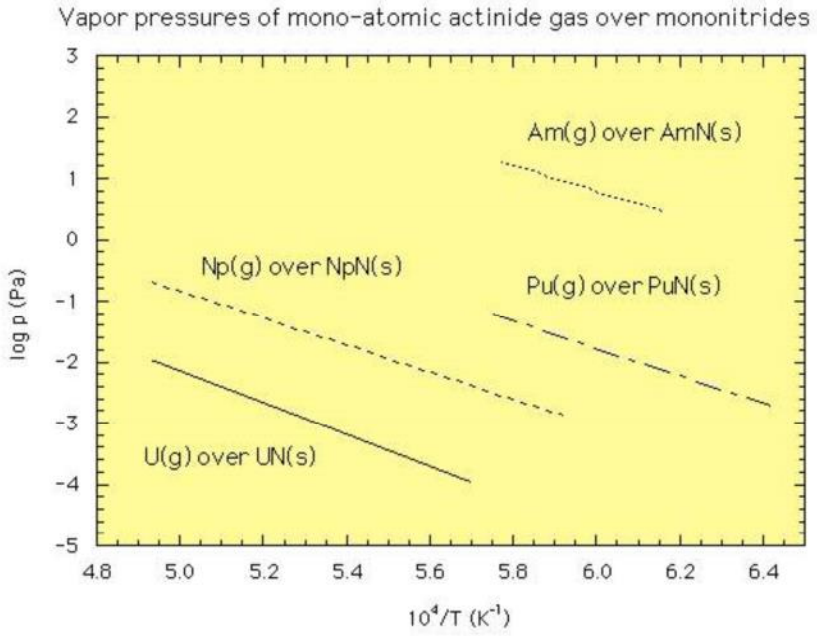

Fig. 2-8-1 Equilibrium vapor pressures of U(g), Np(g), Pu(g) and Am(g) over UN, NpN, PuN and AmN

2.8.2 Vapor pressures of U(g) and Pu(g) over (U,Pu)N

Temperature and composition dependences of equilibrium vapor pressures of U(g) and Pu(g), $p_{U(g)}$ and $p_{Pu(g)}$, over $(U_{1-x}Pu_x)N$ (x=0.20 and 0.35 for U(g), and x=0.2, 0.35, 0.60 and 0.80 for Pu(g)) solid solutions are reported by Suzuki, et al. [48]. The samples were prepared in the same manner as mentioned in 2.4.3. The results for $p_{U(g)}$ and $p_{Pu(g)}$ are fitted to the following equations.

$(U_{0.80}Pu_{0.20})N$:

$\log p_{U(g)}(Pa) = 10.90 - 26400/T \quad (1793 \leq T(K) \leq 1913)$ (2-8-5)

$\log p_{Pu(g)}(Pa) = 9.86 - 20500/T \quad (1653 \leq T(K) \leq 1933)$ (2-8-6)

$(U_{0.65}Pu_{0.35})N$:

$\log p_{U(g)}(Pa) = 11.03 - 26900/T \quad (1813 \leq T(K) \leq 1833)$ (2-8-7)

$\log p_{Pu(g)}(Pa) = 9.59 - 19600/T \quad (1593 \leq T(K) \leq 1833)$ (2-8-8)

$(U_{0.40}Pu_{0.60})N$:

$\log p_{Pu(g)}(Pa) = 11.14 - 22000/T \quad (1553 \leq T(K) \leq 1773)$ (2-8-9)

$(U_{0.20}Pu_{0.80})N$:

$\log p_{Pu(g)}(Pa) = 10.76 - 21100/T \quad (1553 \leq T(K) \leq 1773)$ (2-8-10)

The same authors evaluated the activities of PuN in $(U_{1-x}Pu_x)N$ from $p_{Pu(g)}$ assuming the congruent evaporation of PuN. Further, those of UN in $(U_{1-x}Pu_x)N$ were evaluated by use of the Gibbs-Duhem treatment. The results shown in Table 2-8-1 suggest that the activity coefficients of UN and PuN are nearly unity in UN-rich region of (U,Pu)N, but considerably deviate from unity in PuN-rich region of (U,Pu)N at 1700 K.

Table 2-8-1 Activities and activity coefficients of UN and PuN in (U,Pu)N at 1700 K

	UN		PuN	
	Activity	Activity coefficients	Activity	Activity coefficients
$(U_{0.80}Pu_{0.20})N$	0.802	1.003	0.195	0.975
$(U_{0.65}Pu_{0.35})N$	0.655	1.008	0.336	0.960
$(U_{0.40}Pu_{0.60})N$	0.460	1.149	0.499	0.832
$(U_{0.20}Pu_{0.80})N$	0.227	1.135	0.674	0.843

2.9 Gibbs free energy of formation

2.9.1 Gibbs free energies of formation of UN, NpN, PuN and AmN

Thermodynamic functions of UN are summarized by Hayes, et al., in which Gibbs free energy of formation, Δ_fG, of UN is fitted to the following equation [9]. Matsui and Ohse also reported Δ_fG of UN [52] and the values in two studies agree well each other below 1800 K.

$$\Delta_fG_{UN}\ (J/mol) = -2.941\times10^5 + 80.98\ T - 0.04640\ T^2 + 3.085\times10^{-6}\ T^3 - 1.710\times10^6 / T \quad (298 < T(K) < 2628) \qquad (2\text{-}9\text{-}1)$$

For NpN, Δ_fG is reported by Nakajima, et al., which is fitted to the following equation [49].

$$\Delta_fG_{NpN}\ (J/mol) = -2.959\times10^5 + 89.88\ T \quad (1690 < T(K) < 2030) \qquad (2\text{-}9\text{-}2)$$

Matsui and Ohse summarized thermodynamic functions of PuN, in which Δ_fG of PuN is fitted to the following equation [52].

$$\Delta_fG_{PuN}\ (J/mol) = -3.384\times10^5 + 152.0\ T - 0.03146\ T^2 - 5.998\times10^{-6}\ T^3 + 6.844\times10^6 / T \quad (298 < T(K) < 3000) \qquad (2\text{-}9\text{-}3)$$

For AmN, Ogawa, et al. estimated Δ_fG of AmN from the partial pressure of Am(g) over PuN containing 1.3 at% of ^{241}Am generated by decay of ^{241}Pu [50]. The results are fitted to the following equation.

$$\Delta_f G_{AmN}\ (J/mol) = -2.977\times10^5 + 92.05\ T \qquad (298 < T(K) < 1600) \qquad (2\text{-}9\text{-}4)$$

The Gibbs free energies of formation of UN, NpN, PuN and AmN fitted to Eqs. (2-9-1), (2-9-2), (2-9-3) and (2-9-4) are shown in Fig. 2-9-1.

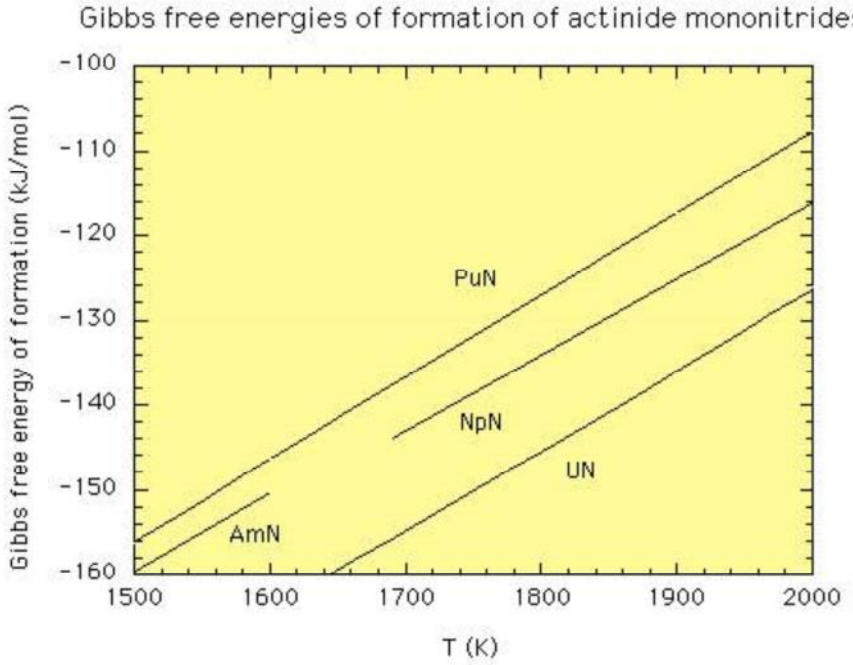

Fig. 2-9-1 Gibbs free energies of formation for UN, NpN, PuN and AmN

2.9.2 Gibbs free energy of formation of (U,Pu)N

Gibbs free energy of formation, $\Delta_f G$, of $(U_{0.8}Pu_{0.2})N$ is given by Matsui and Ohse using an ideal-solution model on UN and PuN [54], which is fitted to the following equation.

$$\Delta_f G_{(U,Pu)N}\ (J/mol) = -2.909\times10^5 + 67.56\ T + 0.007980\ T^2 - 1.098\times10^{-6}\ T^3 - 7.455\times10^5/T$$
$$(298 < T(K) < 3000) \qquad (2\text{-}9\text{-}5)$$

The results reported by Kent and Leary [53] for $\Delta_f G$ of $(U_{0.8}Pu_{0.2})N$ almost agree with those by Matsui and Ohse [52] shown in Fig. 2-9-2.

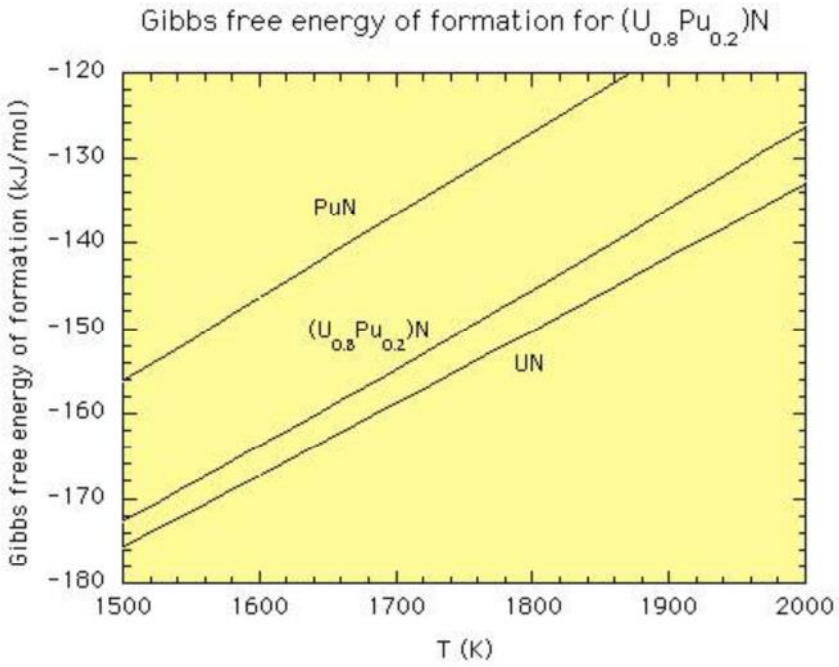

Fig. 2-9-2 Gibbs free energies of formation for $(U_{0.8}Pu_{0.2})N$ besides UN and PuN

2.10 Thermodynamic functions

2.10.1 Standard thermodynamic functions of UN

The standard thermodynamic functions of UN are tabulated by Uno, et al. [15] as shown in Table 2-10-1, using the results reviewed by Hayes, et al. [9], and Matsui and Ohse [52].

Table 2-10-1 Standard thermodynamic functions of UN [14]

T (K)	C_p (J mol^{-1} K^{-1})	$H-H_{298}$ (J mol^{-1})	S (J mol^{-1} K^{-1})	$-(G-H_{298})/T$ (J mol^{-1} K^{-1})	$\Delta_f G$ (J mol^{-1})
298	47.95	0	62.68	62.68	−270 978
300	48.04	96	63.00	62.68	−270 812
400	51.49	5089	77.34	64.62	−262 582
500	53.64	10 352	89.08	68.37	−254 530
600	55.27	15 801	99.01	72.67	−246 614
700	56.63	21 397	107.63	77.06	−238 788
800	57.84	27 121	115.27	81.37	−231 011
900	58.98	32 963	122.15	85.53	−223 235
1000	60.06	38 915	128.42	89.51	−215 267
1100	61.12	44 975	134.19	93.31	−206 948
1200	62.18	51 140	139.56	96.94	−198 457
1300	63.28	57 413	144.57	100.41	−190 019
1400	64.47	63 799	149.28	103.71	−181 626
1500	65.81	70 312	153.74	106.87	−172 640
1600	67.38	76 969	157.98	109.87	−163 550
1700	69.27	83 798	162.01	112.72	−154 384
1800	71.59	90 837	165.87	115.41	−145 111
1900	74.40	98 132	169.58	117.93	−135 687
2000	77.81	105 738	173.14	120.28	−126 062
2100	81.86	113 716	176.58	122.43	−116 178
2200	86.62	122 133	179.90	124.39	−105 969
2300	92.11	131 063	183.12	126.14	−95 367
2400	98.35	140 580	186.24	127.67	−84 302
2500	105.33	150 757	189.28	128.98	−72 701
2600	113.04	161 669	192.23	130.05	−60 489
2628	115.32	164 866	193.04	130.31	−56 954

2.10.2 Standard thermodynamic functions of PuN

The standard thermodynamic functions of PuN are tabulated by Uno, et al. [15] as shown in Table 2-10-2, using the results reviewed by Matsui and Ohse [52].

2.10.3 Standard thermodynamic functions of (U,Pu)N

The standard thermodynamic functions of $(U_{0.8}Pu_{0.2})N$ are tabulated by Uno, et al. [15] as shown in Table 2-10-3, using the results reviewed by Matsui and Ohse [52].

Table 2-10-2 Standard thermodynamic functions of PuN [15]

T (K)	C_p (J mol^{-1} K^{-1})	$H-H_{298}$ (J mol^{-1})	S (J mol^{-1} K^{-1})	$-(G-H_{298})/T$ (J mol^{-1} K^{-1})	$\Delta_f G$ (J mol^{-1})
298	49.60	0	64.81	64.81	−273 247
300	49.63	92	65.12	64.81	−273 073
400	51.17	5132	79.61	66.78	−264 338
500	52.71	10 326	91.19	70.54	−254 777
600	54.26	15 674	100.94	74.81	−245 152
700	55.80	21 177	109.42	79.16	−235 469
800	57.34	26 834	116.97	83.43	−225 714
900	58.88	32 645	123.81	87.54	−215 918
1000	60.42	38 610	130.09	91.48	−205 913
1100	61.97	44 729	135.92	95.26	−195 883
1200	63.51	51 003	141.38	98.88	−185 888
1300	65.05	57 430	146.53	102.35	−175 923
1400	66.59	64 012	151.40	105.68	−166 005
1500	68.13	70 749	156.05	108.88	−156 135
1600	69.68	77 639	160.50	111.97	−146 323
1700	71.22	84 685	164.76	114.95	−136 571
1800	72.76	91 884	168.88	117.83	−126 892
1900	74.30	99 237	172.85	120.63	−117 270
2000	75.84	106 744	176.70	123.33	−107 730
2100	77.38	114 405	180.44	125.96	−98 274
2200	78.93	122 221	184.08	128.52	−88 895
2300	80.47	130 191	187.62	131.02	−79 594
2400	82.01	138 314	191.08	133.45	−70 388
2500	83.55	146 593	194.46	135.82	−61 269
3000	91.26	190 296	210.37	146.94	−17

Table 2-10-3 Standard thermodynamic functions of $(U_{0.8}Pu_{0.2})N$ [15]

T (K)	C_p (J mol^{-1} K^{-1})	$H-H_{298}$ (J mol^{-1})	S (J mol^{-1} K^{-1})	$-(G-H_{298})/T$ (J mol^{-1} K^{-1})	$\Delta_f G$ (J mol^{-1})
298	48.18	0	67.07	67.07	−272 623
300	48.26	96	67.39	67.07	−272 463
400	51.46	5172	83.85	70.92	−264 527
500	53.57	10 354	93.47	72.77	−256 576
600	55.24	15 796	103.39	77.07	−248 723
700	56.71	21 395	112.02	81.45	−240 926
800	58.07	27 134	119.68	85.76	−233 156
900	59.37	33 007	126.60	89.92	−225 395
1000	60.63	39 007	132.92	93.91	−217 422
1100	61.87	45 184	138.91	97.83	−209 381
1200	63.12	51 433	144.35	101.49	−201 030
1300	64.35	57 806	149.45	104.98	−192 746
1400	65.57	64 302	154.26	108.33	−184 520
1500	66.79	70 921	158.83	111.55	−175 853
1600	68.01	77 661	163.18	114.64	−167 164
1700	69.22	84 522	167.34	117.62	−158 499
1800	70.43	91 505	171.33	120.49	−149 859
1900	71.64	98 608	175.17	123.27	−141 237
2000	72.85	105 832	178.87	125.96	−132 654
2100	74.05	113 177	182.45	128.56	−124 114
2200	75.26	120 643	185.93	131.09	−115 614
2300	76.46	128 228	189.30	133.55	−107 156
2400	77.66	135 935	192.58	135.94	−98 723
2500	78.87	143 761	195.77	138.27	−90 365
3000	84.87	184 696	210.68	149.12	−45 975

2.11 Mechanical properties

2.11.1 Young's modulus, shear modulus, bulk modulus and Poisson ratio of UN, U(C,N), (U,Pu)N and (U,Pu)(C,N)

Reports on mechanical properties on actinide nitrides are very limited except for UN. Matzke [1] summarized available elastic properties of UN, U(C,N), (U,Pu)N and (U,Pu)(C,N) at room temperature as shown in Table 2-11-1 [54-59]. Porosity dependence is given for Young modulus only, in which P is the fractional porosity.

Table 2-11-1 Elastic moduli (Young's, shear and bulk modulus) and Poisson ratio at room temperature

Material	Moduli (in GPa)			Poisson	Ref.
	Young's, E	shear, G	bulk, K	ratio, v	
UN	262 (1-2.27 P)	103.7	184.2	0.263	[54]
UN	267 (1-2.7 P)	103.9	205.9	0.284	[55]
UN	265	104.2	191.5	0.272	[56]
$UC_{0.5}N_{0.5}$	245.7	98.0	165.8	0.253	[57]
$(U_{0.85}Pu_{0.15})N$	280 (1-2.7 P)	110	205	0.27	[57,58]
$(U_{0.85}Pu_{0.15})C_{0.85}N_{0.15}$	188.8 [a)]	74.7 [a)]	134 [a)]	0.265 [a)]	[57,59]

[a)] For a specimen with 91.3%TD

On the other hand, Hayes, et al. summarized the experimental data of E, G, K and v of UN and suggested the following fitting equations as a function of temperature T (K) and density D (%TD) [7].

$$E(MPa) = 2.58\times10^{-1}\, D^{3.002}\,(1-2.375\times10^{-5}\, T) \quad (298\le T(K)\le 1473,\ 70\le D(\%TD)\le 100) \quad (2\text{-}11\text{-}1)$$

$$G(MPa) = 1.44\times10^{-2}\, D^{3.446}\,(1-2.375\times10^{-5}\, T) \quad (298\le T(K)\le 1473,\ 70\le D(\%TD)\le 100) \quad (2\text{-}11\text{-}2)$$

$$K(MPa) = 1.33\times10^{-3}\, D^{4.074}\,(1-2.375\times10^{-5}\, T) \quad (298\le T(K)\le 1473,\ 70\le D(\%TD)\le 100) \quad (2\text{-}11\text{-}3)$$

$$v = 1.26\times10^{-3}\, D^{1.174} \quad (298\le T(K)\le 1473,\ 70\le D(\%TD)\le 100) \quad (2\text{-}11\text{-}4)$$

Thetford, et al. assumed the following equations for the temperature dependence of E and G of (U,Pu,Zr)N in their modeling study [60]. P in the equations denotes the fractional porosity.

$$E(GPa) = 280\,(1.0274 - 0.92\times10^{-4}\, T)\,(1 - 2.7\, P) \quad (2\text{-}11\text{-}5)$$

$$G(GPa) = 110\ (1.0274 - 0.92\times10^{-4}\,T)\ (1 - 2.62\,P) \qquad (2\text{-}11\text{-}6)$$

2.11.2 Hardness of UN, PuN, (U,Pu)N, U(C,N) and (U,Pu)(C,N)

Table 2-11-2 shows the Vickers hardness of UN, PuN, (U,Pu)N, U(C,N) and (U,Pu)(C,N) at room temperature [1,61-65] summarized by Matzke [1]. The temperature dependence of the Vickers hardness of UN, PuN and $(U_{0.7}Pu_{0.3})N$ is also briefly mentioned [1].

It should be noted that the hardness data of ceramics measured by the Vickers-diamond indentation are influenced by microstructure and impurity contents, and these effects are particularly important at high temperature. Also the load dependence is often observed.

Table 2-11-2 Vickers hardness data of UN, PuN, (U,Pu)N, U(C,N) and (U,Pu)(C,N) at room temperature

Material	H (GPa)	Load (N)	Ref.
UN	4.6	15.1	[61]
$(U_{0.7}Pu_{0.3})N$	5.1	98.1	[62]
$(U_{0.8}Pu_{0.2})N$	6.6	0.49-1.96	[63]
PuN	3.3, 4.7	1.96	[64], [65]
$U(C_{1-x}N_x)$	6.5 (x=1) ~ 9 (x=0.5)	0.49	[1]
$(U_{0.8}Pu_{0.2})(C_{1-x}N_x)$	5.5 (x=1) ~ 11 (x=0)	0.49	[1]

On the other hand, Hayes, et al., summarized the experimental hardness data of UN and suggested the following fitting equation as a function of temperature T(K) and porosity P [7].

$$HD\ (kg/mm^2) = 951.8\ (1\text{-}2.1\,P)\ \exp(-1.882\times10^{-3}\,T) \quad (298\le T(K)\le1673,\ 0\le P\le0.26) \qquad (2\text{-}11\text{-}7)$$

2.11.3 Thermal creep of UN, U(C,N) and (U,Pu)(C,N)

Limited creep data exist for UN, U(C,N) and (U,Pu)(C,N) and they are summarized by Matzke [1]. Quite generally, the steady state creep rate, $\dot{\varepsilon}=d\varepsilon/dt$, in which ε is the measured length change of specimen, is a function of the applied stress σ, temperature T, composition of the specimen, grain size d, and orientation in case of a single crystal. The steady state creep rate is described in terms of the following simplified empirical equation.

$$\dot{\varepsilon} = A\,\sigma^n \exp(-\Delta H/RT) \qquad (2\text{-}11\text{-}8)$$

where A and n are constants at a constant composition and structure. Hayes, et al.

suggested that $A(h^{-1})=7.39$, $n=4.5$ and $\Delta H(kJ/mol)=326.8$ for UN and the following porosity correction factor [7].

$$f(P) = \{0.987 / (1-P)^{27.6}\} \exp(-8.65P) \qquad (2\text{-}11\text{-}9)$$

But the existing creep data for actinide nitrides are not so clear and not quantitatively understood at present. A dependence of creep rate on nitrogen partial pressure may also exist. Matzke concluded that it is premature to suggest equations for nitride fuel at present [1].

Thetford, et al. assumed the creep rate of (U,Pu,Zr)N as the following equation in their modeling study [60].

$$\dot{\varepsilon}\ (s^{-1}) = \exp(25P)\ [6.46\times10^{-6}\ \sigma^{6} \exp(-37750/T) + 5.33\times10^{-32}\ \sigma F'] \qquad (2\text{-}11\text{-}10)$$

where P is the porosity and F' is the fission rate (fissions/m^3/s).

Besides, the creep data of UN, (U,Nd)N and (U,Zr)N measured by micro-indentation technique exist in JAEA. It is suggested that the addition of Nd or Zr to UN results in lowering creep rates as shown in Fig. 2-11-1 [66].

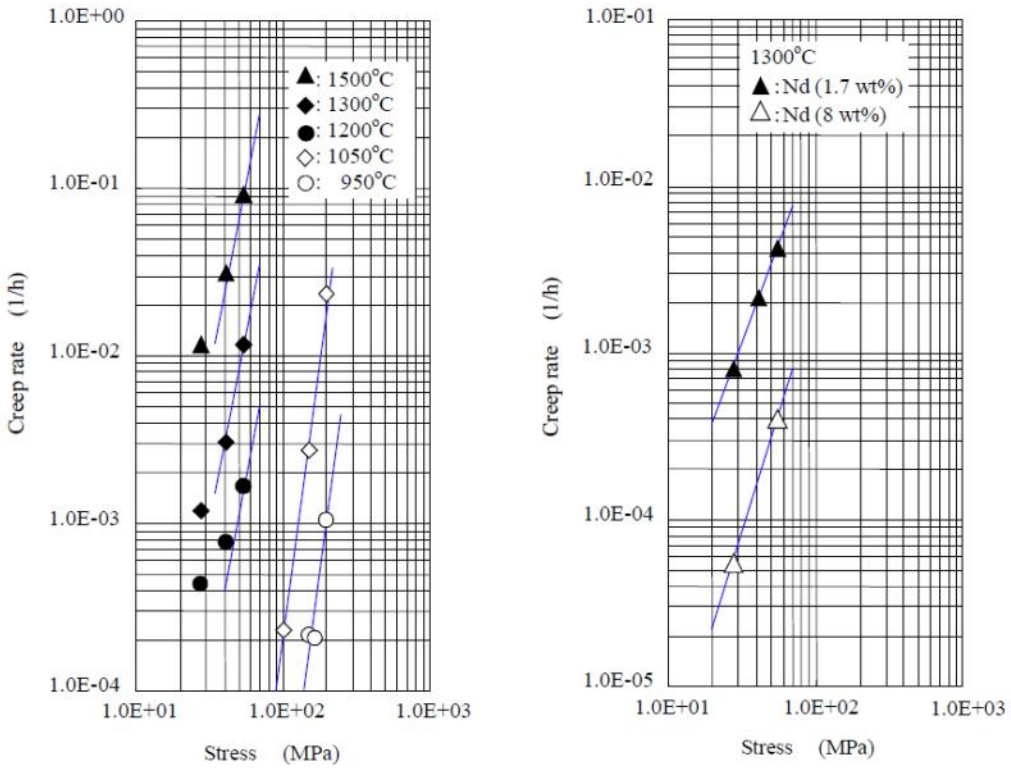

Fig. 2-11-1 Thermal creep rates of UN (left) and (U,Nd)N (right) measured by micro-indentation technique

2.11.4 Thermal and irradiation creep of UN

Thermal creep predominates at high temperatures, while irradiation creep predominates at low temperatures in UN [14]. The thermal creep rate of UN, $\dot{\varepsilon}_T(s^{-1})$, is calculated from the following equation as a function of temperature T(K), gap pressure σ(MPa) and porosity P, which is suggested by Hayes, et al. [7].

$$\dot{\varepsilon}_T = 2.054\times10^{-3}\ \sigma^{4.5} \exp(-39369.5/T) \times \{0.987 \exp(-8.65P) / (1-P)^{27.6}\} \qquad (2\text{-}11\text{-}11)$$

The solid line in Fig. 2-11-2 shows the calculated thermal creep rate of UN, assuming σ=20 MPa and P=0.15

On the other hand, the irradiation creep rate of UN, $\dot{\varepsilon}_I(s^{-1})$, is calculated from the following equation as a function of gap pressure σ(MPa), porosity P and fission rate density f(fissions/cm^3/s), which is suggested by Billone, et al. [67].

$$\dot{\varepsilon}_I = 1.81\times10^{-26}\ (1 + 1250\ P^2)\ f\ \sigma \qquad (2\text{-}11\text{-}12)$$

The dashed line in Fig. 2-11-2 shows the calculated irradiation creep rate of UN, assuming σ=20 MPa, P=0.15 and f=10^{13} fissions/cm^3/s.

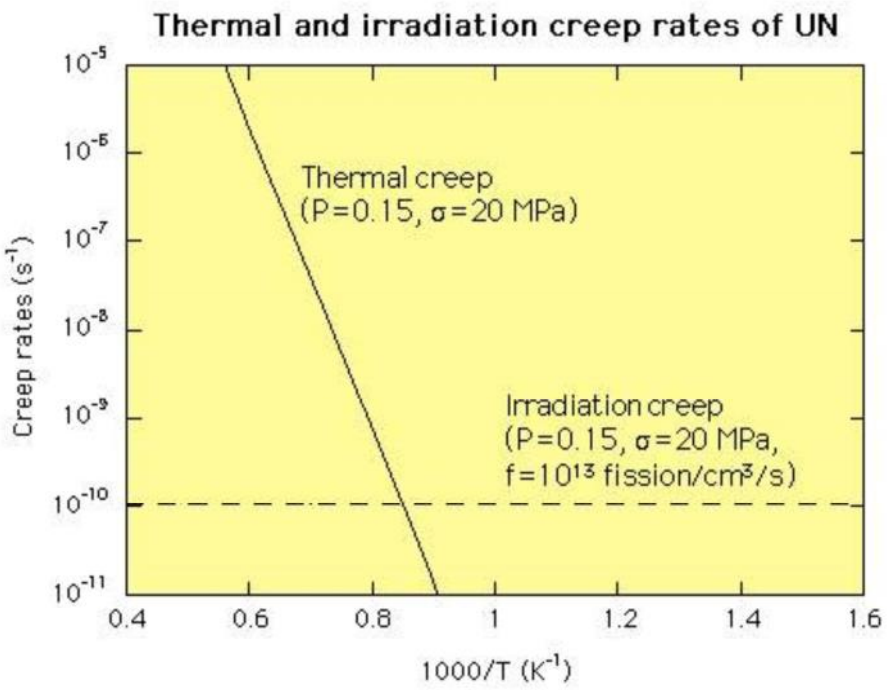

Fig. 2-11-2 Thermal and irradiation creep rates of UN
at P=0.15, σ=20 MPa, f=10^{13} fissions/cm^3/s

2.12 Diffusion characteristics

2.12.1 Nitrogen diffusion in UN

Existing data for nitrogen diffusion in UN show a pronounce dependence on nitrogen partial pressure. These results indicate an interesting mechanism for nitrogen diffusion showing the dependence on the square root of nitrogen partial pressure [12]. The non-metal atom diffusion is considerably slower in UN than in UC. Data for nitrogen diffusion in PuN and (U,Pu)N are not available.

On the other hand, Hayes, et al. suggested the following Arrhenius equation for nitrogen diffusion in UN [8],

$$D_{N\ in\ UN}\ (cm^2/s) = 2.252\times10^{-5}\ P_N^{0.4134}\ g^{-0.737+2.179\times10^{-4}\ T}\ \exp(-19214.7/T) \quad (2\text{-}12\text{-}1)$$

where T is temperature in K, P_N is nitrogen pressure in atm and g is grain size in μm.

2.12.2 Pu diffusion in (U,Pu)N and U diffusion in UN

Data for Pu diffusion in (U,Pu)N are collected by applying the so-called "α-energy degradation method", in which α-particles emitted from Pu atom lose energy by ionization on their way to the surface, thus giving rise to counts in the energy spectrum at lower energy. The following Arrhenius equations for Pu diffusion in (a) $(U_{0.81}Pu_{0.19})N_{1.01}C_{0.01}O_{0.09}$ and (b) $(U_{0.81}Pu_{0.19})N_{0.98}C_{0.01}O_{0.04}$ are reported, respectively [1]. These results were obtained at a constant nitrogen pressure ($p(N_2)$=53 kPa) and therefore not at a constant composition.

$$\text{(a) } D_{Pu\ in\ (U,Pu)N}\ (cm^2/s) = 0.019\ \exp(-107600/RT) \quad (2\text{-}12\text{-}2)$$

$$\text{(b) } D_{Pu\ in\ (U,Pu)N}\ (cm^2/s) = 0.25\ \exp(-118600/RT) \quad (2\text{-}12\text{-}3)$$

where R is gas constant and Tis temperature in K. Nitrogen partial pressure dependences of $D_{Pu\ in\ (U,Pu)N}$ at three different temperatures are also reported [1]. At 1923K, a relation $D_{Pu\ in\ (U,Pu)N} \propto p(N_2)^{1/n}$ with n=4.2, whereas at 1993 and 2083K, n=6.8 and n=200, respectively. $D_{Pu\ in\ (U,Pu)N}$ becomes practically independent of $p(N_2)$ at higher temperatures.

Reliable experimental data for U diffusion in UN are lacking. However, Hayes, et al. suggested the following Arrhenius equation for U diffusion in UN [8].

$$D_{U\ in\ UN}\ (cm^2/s) = 2.215\times10^{-11}\ P_N^{0.6414}\ \exp(-7989.3/T) \quad (2\text{-}12\text{-}4)$$

where T is temperature in K and P_N is nitrogen pressure in atm.

2.12.3 Fission gas atom diffusion in UN and (U,Pu)N

The fission gas atom diffusion coefficient D (cm^2/s) is proposed as the following equation with an additional burnup factor F_B by Weinstein, et al. [68].

$$D = F_B\ 8.22\times10^{-31}\ f + 2.37\times10^{-30}\ \exp(-18800/T) + 10^{-18}\ f\ \exp(-18400/T)/K^2T^2 \qquad (2\text{-}12\text{-}5)$$

where f is the fission rate density ($fissions/cm^3/s$), K is the thermal conductivity (W/cm/K) and T is the temperature (K). This equation is derived based on measurements of ^{88}Kr from the irradiated UN fuel pins at 6% burnup and assumes complete interconnection of circumferential intergranular porosity, which is appropriate for high as-fabricated porosity. The burnup factor F_B takes into account the effect of fission product accumulation which is more pronounced on the low temperature components of the diffusion coefficient.

$$F_B = 30 + BU \qquad (2\text{-}12\text{-}6)$$

where BU is the burnup (MWd/kg).

On the other hand, Thetford, et al. recommend the following equation of inert gas atom diffusion in (U,Pu)N in their modeling study [60], which is derived from the Xe diffusion data by Blank [12].

$$D_{Xe,\ nitride}\ (m^2/s) = 1.143\times10^{-7}\ \exp(-35225/T) \qquad (2\text{-}12\text{-}7)$$

where T is temperature in K.

2.13 Fission gas release

2.13.1 Fission gas release of UN and (U,Pu)N

Storms suggested the following fitting equation of fission gas release R (%) of UN and (U,Pu)N as a function of temperature T (K), burnup B (at%) and theoretical density TD (%) by summarizing 95 experimental data sets of UN and 39 experimental data sets of (U,Pu)N, for up to T=2000 K, up to B=20 at% and for 80<TD(%)<97 [10].

$$R = 100 / [\exp\{0.0025\ (90\ TD^{0.77}/\ B^{0.09} - T)\} + 1] \qquad (2\text{-}13\text{-}1)$$

The standard deviation and the average fractional error of R (%) are evaluated at 3.2 and -2.8, respectively.

Bauer, et al. noted from their irradiation data of (U,Pu)N that fission gas release rate (%/%FIMA) increases drastically (~20 times higher) when fuel porosity increases from 10% to 20% [68]. This was explained by the change of mechanism from recoil release to release

through surface connected porosity.

Fig. 2-13-1 shows the fission gas release rate of UN calculated from Eq. (2-13-1) assuming that T=1473 K and TD=85% or 95%.

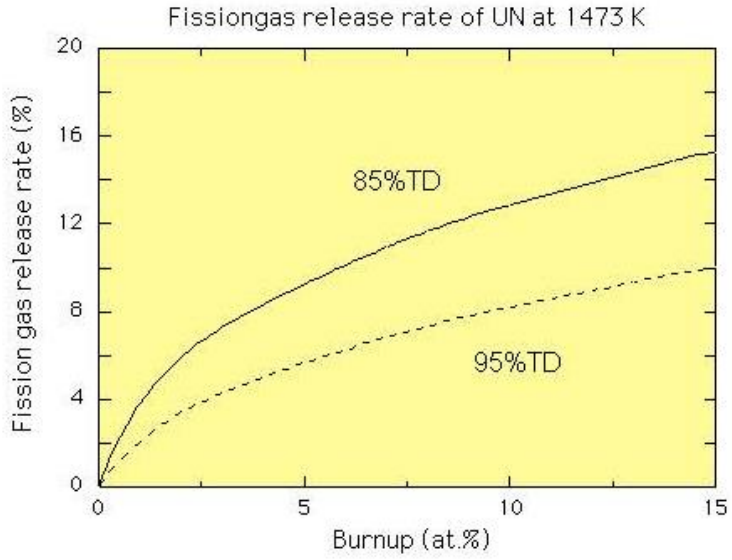

Fig. 2-13-1 Fission gas release rate of UN

2.14 Swelling characteristics

2.14.1 Swelling of UN and (U,Pu)N

Mechanism of swelling of nitride fuel, as well as carbide fuel and carbonitride fuel, was investigated in detail in ITU [1,12]. The goal of the study, “Swelling of Advanced Fuels”, was clarification of basic processes contributing to swelling, being discussed with the fuel structure and fuel temperature. A critical temperature, above which fission gas bubble swelling accelerates, for (U,Pu)N was estimated at about 1573-1673 K.

Bauer, et al. also summarized the measured swelling rates of nitride fuel and suggested the similar critical temperature for both low-density (<84%TD) and high-density (>94%TD) fuel pellets [68]. Below the critical temperature, a swelling rate of around 1%ΔV/V per at% burnup is recommended for (U,Pu)N in general.

Ross, et al. proposed the following fitting equation of swelling of UN fuel with Nb-1%Zr and PWC-11 cladding tubes (namely, restrained swelling with cladding tube) as a function of volume averaged fuel temperature T_{av} (K), fuel burnup B (at%) and fuel density TD (% of theoretical density) [11].

$$\Delta V/V\ (\%) = 4.7\times10^{-11}\ T_{av}^{3.12}\ B^{0.83}\ TD^{0.5} \qquad (2\text{-}14\text{-}1)$$

Eq. (2-14-1) can be written in terms of maximum fuel temperature T_m as following.

$$\Delta V/V\ (\%) = 1.16\times10^{-8}\ T_m^{2.36}\ B^{0.82}\ TD^{0.5} \qquad (2\text{-}14\text{-}2)$$

The uncertainties of these restrained swelling correlations are within ± 25 % at B > 1.12 at%. Those at lower burnups (B < 1.12 at%) results in a deviation as high as ± 60 %.

On the other hand, the fitting equation for unrestrained swelling (namely, swelling without cladding tube) is not available for UN and (U,Pu)N. The following equation proposed by Zimmermann shows the results for (U,Pu)C fuel at 500 ≤ T(K) ≤ 2000 [69].

$$S = 0.8\ B + C_1\ \{1 - \exp(-C_2\ B)\} \qquad (2\text{-}14\text{-}3)$$

$$C_1 = 10 + 24 / [1 + \exp\{(1400\text{-}T)/74\}]$$

$$C_2 = 0.06 + 8.25\times10^3\ \exp\{(-2.027\times10^4)/T\}$$

$$T = (1 - t_{Tmax}/t)\ T_m + (t_{Tmax}/t)\ T_{max}$$

where S is the unrestrained swelling (vol.%), B is the burnup (%), T is the Fuel temperature (K), T_m is the time-averaged temperature (K), T_{max} is the maximum fuel temperature (K), t is the irradiation period and t_{Tmax} is the time at which maximum fuel temperature is observed.

3. Summary

Published data from JAEA as well as from other organizations on properties of TRU nitrides are summarized as a “Property Database of TRU Nitride Fuel”. The collected and evaluated data cover the properties needed for the design of ADS. As mentioned in the Introduction, property data on TRU nitrides are often lacking. In such cases, those on UN and (U,Pu)N are substitutionally shown in order to complement the database and facilitate the design with tolerable accuracy. Data are formulated as functions of composition, temperature, density, etc. as much as possible for corresponding to a variety of conditions. The present database will be useful to not only the design of ADS but also planning and licensing irradiation tests for demonstrating the fuel performance of ADS and potential advanced reactors with nitride fuel.

Although we can obtain the results of post-irradiation examination (PIE) of UN and (U,Pu)N carried out so far, TRU nitride fuels may show some different irradiation behavior from those of UN and (U,Pu)N. As the next step, the irradiation tests of TRU nitride fuels are planned in JAEA in order to contribute to the advance of fuel design and the demonstration of fuel performance of ADS.

Acknowledgements

The authors wish to express their thanks to Drs. M. Chino, M. Yamamoto, K. Minato and M. Akabori for the interest in this study and invaluable suggestions.

References

[1] Matzke, H. J., Science of Advanced LMFBR Fuels, North-Holland, 1986, 740p.
[2] Matthews, R. B. et al., Fabrication and Testing of Uranium Nitride Fuel for Space Power Reactors, J. Nucl. Mater., vol. 151, 1988, pp. 334-344.
[3] Tsujimoto, K. et al., Neutronics Design for Lead-bismuth Cooled Accelerator-driven System for Transuranium of Minor Actinide, J. Nucl. Sci. Technol., vol. 41, 2004, pp. 21-36.
[4] Besmann, T. M. et al., Fission Product Release and Survivability of UN-kernel LWR TRISO Fuel, J. Nucl. Mater., 2014, doi:10.1016/ j.jnucmat.2013.10.034.
[5] Takano, M., Preparation of Nitride Fuel Pellet with TiN Inert Matrix for Transmutation of Minor Actinides, Proceedings of GLOBAL 2011, Makuhari, Japan, 2011, 6p. in CD-ROM.
[6] Hayes, S. L. et al., Material Property Correlations for Uranium Mononitride I. Physical Properties, J. Nucl. Mater., vol. 171, 1990, pp. 262-270.
[7] Hayes, S. L. et al., Material Property Correlations for Uranium Mononitride II. Mechanical Properties, J. Nucl. Mater., vol. 171, 1990, pp. 271-288.
[8] Hayes, S. L. et al., Material Property Correlations for Uranium Mononitride III. Transport Properties, J. Nucl. Mater., vol. 171, 1990, pp. 289-299.
[9] Hayes, S. L. et al., Material Property Correlations for Uranium Mononitride IV. Thermodynamic Properties, J. Nucl. Mater., vol. 171, 1990, pp. 300-318.
[10] Storms, E. K., An Equation which Describes Fission Gas Release from UN Reactor Fuel, J. Nucl. Mater., vol. 158, 1988, pp. 119-129.
[11] Ross, S. B. et al., Uranium Nitride Fuel Swelling Correlation, J. Nucl. Mater., vol. 170, 1990, pp. 169-177.
[12] Blank, H., Nonoxide Ceramic Nuclear Fuels, Materials Science and Technology, vol. 10A, eds. Cahn, R. W. et al., VCH, 1994, pp. 191-363.
[13] Kim, Y. S. et al., AAA Fuel Handbook, ANL-AAA-068, 2003, 215p.
[14] Feng, B. et al., Steady-state Fuel Behavior Modelling of Nitride Fuels in FRAPCON-EP, J. Nucl. Mater., vol. 427, 2012, pp. 30-38.
[15] Uno, M. et al., Thermodynamic and Thermophysical Properties of the Actinide Nitrides, Comprehensive Nuclear Materials, eds. Konings, R. J. M. et al., Elsevier, vol. 2, 2012, pp. 61-85.
[16] Benedict, U., Structural Data of the Actinide Elements and of Their Binary Compounds with Non-Metallic Elements, J. Less-Common Met., vol. 128, 1987, pp. 7-45.
[17] Takano, M., Experimental Evaluation of Solid Solubility of Lanthanide and

Transuranium Nitride into ZrN Matrix, J. Nucl. Mater., vol. 440, 2013, pp. 489-494.
[18] Sheth, A. et al., Equation of State and Transport Properties of Uranium and Plutonium Nitrides in the Liquid Region, ANL-AFP-12, 1975, 32p.
[19] Okamoto, Y. et al., Self-irradiation damage in PuN, J. Nucl. Mater., vol. 206, 1993, pp. 94-96.
[20] Shimbarev, E. V. et al., Synthesis and Study of Binaly Compounds of Actinides and Lanthanides. V. Influence of Internal Irradiation on Crystal Lattice of Americium-241 Nitride, Radiokhimya, vol. 26, 1984, pp. 643-645.
[21] Takano, M. et al., Thermal Expansion and Self-irradiation Damage in Curium Nitride Lattice, J. Nucl. Mater., 2014, doi:10.1016/j.jnucmat.2014.01.042.
[22] Oetting, F. L., The Chemical Thermodynamic Properties of Nuclear Materials III. Plutonium Mononitride, J. Chem. Thermodyn., vol. 10, 1978, pp. 941-948.
[23] Nishi, T. et al., Heat Capacity of NpN and AmN, J. Nucl. Mater., vol. 377, 2008, pp. 467-469.
[24] Alexander, C. A. et al., Thermodynamic Properties of (U,Pu)N, Nucl. Metallurgy, vol. 17, 1970, pp. 95-103.
[25] Pukari, M. et al., Sintering and Characterization of (Pu,Zr)N, J. Nucl. Mater., vol. 444, 2014, pp. 421-427.
[26] Nishi, T. et al., Thermal Conductivities of Zr-based Transuranium Nitride Solid Solutions, J. Nucl. Sci. Technol., vol. 48, 2011, pp. 359-365.
[27] Barin, I., Thermochemical Data of Pure Substances Third Edition, 1995, p.1878.
[28] Schulz, B., Thermal Conductivity of Porous and Highly Porous Materials, High Temp. -High Press., vol. 13, 1981, pp. 649-660.
[29] Bakker, K. et al., The Contribution of Thermal Radiation to the Thermal Conductivity of Porous UO_2, J. Nucl. Mater. vol. 223, 1995, pp. 135-142.
[30] Morimoto, K. et al., Recovery Behaviors of Thermal Conductivities in Self-irradiated MOX-fuel, IOP Conf. Series: Mater. Sci. Eng., vol. 9, 2010, 012008.
[31] Arai, Y. et al., Dependence of the Thermal Conductivity of (U,Pu)N on Porosity and Plutonium Content, J. Nucl. Mater., vol. 195, 1992, pp. 37-43.
[32] Arai, Y. et al., Thermal Conductivity of Neptunium Mononitride from 740 to 1600 K, J. Nucl. Mater., vol. 211, 1994, pp. 248-250.
[33] Nishi, T. et al., Thermal Conductivities of Neptunium and Americium Mononitride, Proceedings of 10th OECD/NEA Information Exchange Meeting on Actinide and Fission Product Partitioning and Transmutation, Mito, Japan, 2010, 8p. in CD-ROM.
[34] Basini, V. et al., Experimental Assessment of Thermophysical Properties of (Pu,Zr)N, J. Nucl. Mater., vol. 344, 2005, pp. 186-190.
[35] Ciriello, A. et al., Thermophysical Characterization of ZrN and (Zr,Pu)N, J. Alloys Comp., vol. 473, 2009, pp. 265-271.

[36] Arai, Y. et al., Thermal Conductivity of Actinide Mononitride Solid Solutions, J. Alloys Comp., vol. 271-273, 1998, pp. 602-605.
[37] Nishi, T. et al., Thermal Conductivities of (Np,Am)N and (Pu,Am)N Solid Solutions, IOP Conf. Ser. Mater. Sci. Eng., vol. 9, 2010, 012017.
[38] Nishi, T. et al., Thermal Conductivity of Minor Actinide Nitride Solid Solutions, AESJ 2008 Spring Meeting, G-26, 26-28 March, 2008, Osaka, Japan.
[39] Takano, M. et al., Lattice Thermal Expansions of NpN, PuN and AmN, J. Nucl. Mater., vol. 376, 2008, pp. 114-118.
[40] Takano, M. et al., Thermal Expansion of TRU Nitride Solid Solutions as Fuel Materials for Transmutation of Minor Actinides, J. Nucl. Mater., vol. 389, 2009, pp. 89-92.
[41] Costa, P. et al., Magnetic Transitions in Uranium and Plutonium Mononitrides, Monocarbides and Sesquicarbides, Compounds of Interests in Nuclear Reactor Technology, eds. Weber, J. T. et al., AIME, 1964, pp. 83-91.
[42] Keller, D. L., Annual Report - Progress Relating to Civilian Applications during July 1966 through June 1967, BMI-1809, 1967, 206p.
[43] Erdős, P. et al., The Physics of Actinide Compounds, Plenum Press, 1983, p.14.
[44] Olson, W. M. et al., The Decomposition Pressure and Melting Point of Uranium Mononitride, J. Phys. Chem., vol. 67, 1963, pp. 952-954.
[45] Olson, W. M. et al., The Melting Point and Decomposition Pressure of Neptunium Mononitride, J. Phys. Chem., vol. 70, 1966, pp. 2932-2934.
[46] Olson, W. M. et al., The Decomposition Pressure and Melting Point of Thorium Mononitride, J. Phys. Chem., vol. 68, 1964, pp. 1048-1051.
[47] Spear, K. E. et al., Review and Analysis of Phase Behavior and Thermodynamic Properties of the Plutonium-Nitrogen System, ORNL-TM-2106, 1968, 24p.
[48] Suzuki, Y. et al., Vaporization Behavior of Uranium-Plutonium Mixed Nitride, J. Nucl. Mater., vol. 188, 1992, pp. 239-243.
[49] Nakajima, K. et al., Vaporization Behavior of Neptunium Mononitride, J. Nucl. Mater., vol. 247, 1997, pp. 33-36.
[50] Takano, M. et al., Study on The Stability of AmN and (Am,Zr)N, Proceedings of GLOBAL 2003, New Orleans, USA, 2003, pp. 2285-2291 in CD-ROM.
[51] Ogawa, T. et al., Vaporization Behavior of (Pu,Am)N, J. Alloys Compd., vol. 224, 1995, pp. 55-59.
[52] Matsui, T. et al., Thermodynamic Properties of Uranium Nitride, Plutonium Nitride and Uranium-Plutonium Mixed Nitride, High Temp. High Press., vol. 19, 1987, pp. 1-17.
[53] Kent, R. A. et al., Mass Spectrometric Studies of Plutonium Compounds at High Temperature, High Temp. Sci., vol. 1, 1969, pp. 176-183.
[54] Whaley, H. L. et al., Elastic Moduli and Debye Temperature of Polycrystalline Uranium Nitride by Ultrasonic Velocity Measurements, J. Nucl. Mater., vol. 31, 1969, pp.

345-350.
[55] Padel, A. et al., Constantes Elastiques des Carbures, Nitrures et Oxydes D'uranium et de Plutonium, J. Nucl. Mater., vol. 33, 1969, pp. 40-51.
[56] Guinan, U. et al., Elastic Properties of Uranium Mononitride at 298 K, J. Nucl. Mater., vol. 43, 1972, pp. 205-206.
[57] Novion, C. H. et al., Mechanical Properties of Plutonium-Based Ceramics at High Temperature. Application to Fuel Elements, CEA-Conf-1670, 1970, 17p.
[58] Novion, C. H. et al., Mechanical Properties of Uranium- and Plutonium-Based Ceramics, Plutonium 1970 and Other Actinides, ed. W.N. Miner, Nucl. Metallurgy, vol. 17 1970, pp. 509-517.
[59] Padel, A. et al., Constantes Elastiques des Carbonitrures D'uranium et de Plutonium $UC_{1-x}N_x$ et $(U_{0.85}Pu_{0.15})(C_{1-x}N_x)$, J. Nucl. Mater., vol. 36, 1970, pp. 297-303.
[60] Thetford, R. et al., The Chemistry and Physics of Modelling Nitride Fuels for Transmutation, J. Nucl. Mater., vol. 320, 2003, pp. 44-53.
[61] Harrison, J. D. L. et al., Factors Affecting the Hardness of Uranium Mononitride, Plutonium 1970 and Other Actinides, ed. W.N. Miner, Nucl. Metallurgy, vol. 17, 1970, pp. 518-529.
[62] French, P. M. et al., Mechanical Properties and Compatibility of Uranium-Plutonium Carbides, Proceedings of Plutonium 1965, London, UK, 1967, pp.697-720.
[63] Matzke, H. J. et al., Fracture-surface Energy and Fracture Toughness of (U,Pu)C and (U,Pu)(C,O), J. Am. Ceram. Soc., vol. 66, 1983, pp. 183-188.
[64] Toker, M. et al., Mechanical Properties of Carbide and Nitride Reactor Fuels, LA-4452, 1970, 9p.
[65] Weber, W. J. et al., Indentation Testing of Nuclear-waste Glasses, J. Mater. Sci., vol. 19, 1984, pp. 2533-2545.
[66] Arai, Y. et al., JAEA's Activities on Nitride Fuel Research for MA Transmutation, Proceedings of 9th OECD/NEA Information Exchange Meeting on Actinide and Fission Product Partitioning and Transmutation, Nimes, France, 2007, pp.117-126.
[67] Billone, M. C. et al., Progress in Modeling Carbide and Nitride Fuel Performance in Advanced LMFBRs, Proceedings of Advanced LMFBR Fuels, Tucson, USA, 1977 pp. 516-536.
[68] Bauer, A. A. et al., Mixed Nitride Fuel Irradiation Performance, Proceedings of ANS Conference on Fast Reactor Fuel Element Technology, New Orleans, USA, 1971, pp. 785-817.
[69] Zimmermann, H., Investigation of Swelling of U-Pu Mixed Carbide, J. Nucl. Mater., vol. 105, 1982, pp. 56-61.

This is a blank page.

国際単位系（SI）

表１．SI 基本単位

基本量	SI 基本単位	
	名称	記号
長さ	メートル	m
質量	キログラム	kg
時間	秒	s
電流	アンペア	A
熱力学温度	ケルビン	K
物質量	モル	mol
光度	カンデラ	cd

表２．基本単位を用いて表されるSI組立単位の例

組立量	SI 基本単位	
	名称	記号
面積	平方メートル	m^2
体積	立法メートル	m^3
速さ，速度	メートル毎秒	m/s
加速度	メートル毎秒毎秒	m/s^2
波数	毎メートル	m^{-1}
密度，質量密度	キログラム毎立方メートル	kg/m^3
面積密度	キログラム毎平方メートル	kg/m^2
比体積	立方メートル毎キログラム	m^3/kg
電流密度	アンペア毎平方メートル	A/m^2
磁界の強さ	アンペア毎メートル	A/m
量濃度(a)，濃度	モル毎立方メートル	mol/m^3
質量濃度	キログラム毎立法メートル	kg/m^3
輝度	カンデラ毎平方メートル	cd/m^2
屈折率(b)	（数字の） 1	1
比透磁率(b)	（数字の） 1	1

(a) 量濃度（amount concentration）は臨床化学の分野では物質濃度（substance concentration）ともよばれる。
(b) これらは無次元量あるいは次元１をもつ量であるが、そのことを表す単位記号である数字の１は通常は表記しない。

表３．固有の名称と記号で表されるSI組立単位

組立量	SI 組立単位			
	名称	記号	他のSI単位による表し方	SI基本単位による表し方
平面角	ラジアン(b)	rad	1 (b)	m/m
立体角	ステラジアン(b)	sr(c)	1 (b)	m^2/m^2
周波数	ヘルツ(d)	Hz		s^{-1}
力	ニュートン	N		m kg s^{-2}
圧力，応力	パスカル	Pa	N/m^2	m^{-1} kg s^{-2}
エネルギー，仕事，熱量	ジュール	J	N m	m^2 kg s^{-2}
仕事率，工率，放射束	ワット	W	J/s	m^2 kg s^{-3}
電荷，電気量	クーロン	C		s A
電位差（電圧），起電力	ボルト	V	W/A	m^2 kg s^{-3} A^{-1}
静電容量	ファラド	F	C/V	m^{-2} kg^{-1} s^4 A^2
電気抵抗	オーム	Ω	V/A	m^2 kg s^{-3} A^{-2}
コンダクタンス	ジーメンス	S	A/V	m^{-2} kg^{-1} s^3 A^2
磁束	ウエーバ	Wb	Vs	m^2 kg s^{-2} A^{-1}
磁束密度	テスラ	T	Wb/m^2	kg s^{-2} A^{-1}
インダクタンス	ヘンリー	H	Wb/A	m^2 kg s^{-2} A^{-2}
セルシウス温度	セルシウス度(e)	℃		K
光束	ルーメン	lm	cd sr(c)	cd
照度	ルクス	lx	lm/m^2	m^{-2} cd
放射性核種の放射能(f)	ベクレル(d)	Bq		s^{-1}
吸収線量, 比エネルギー分与, カーマ	グレイ	Gy	J/kg	m^2 s^{-2}
線量当量, 周辺線量当量, 方向性線量当量, 個人線量当量	シーベルト(g)	Sv	J/kg	m^2 s^{-2}
酸素活性	カタール	kat		s^{-1} mol

(a)SI接頭語は固有の名称と記号を持つ組立単位と組み合わせても使用できる。しかし接頭語を付した単位はもはやコヒーレントではない。
(b)ラジアンとステラジアンは数字の１に対する単位の特別な名称で、量についての情報をつたえるために使われる。実際には、使用する時には記号radおよびsrが用いられるが、習慣として組立単位としての記号である数字の１は明示されない。
(c)測光学ではステラジアンという名称と記号srを単位の表し方の中に、そのまま維持している。
(d)ヘルツは周期現象についてのみ、ベクレルは放射性核種の統計的過程についてのみ使用される。
(e)セルシウス度はケルビンの特別な名称で、セルシウス温度を表すために使用される。セルシウス度とケルビンの単位の大きさは同一である。したがって、温度差や温度間隔を表す数値はどちらの単位で表しても同じである。
(f)放射性核種の放射能（activity referred to a radionuclide）は、しばしば誤った用語で"radioactivity"と記される。
(g)単位シーベルト（PV,2002,70,205）についてはCIPM勧告2（CI-2002）を参照。

表４．単位の中に固有の名称と記号を含むSI組立単位の例

組立量	SI 組立単位		
	名称	記号	SI 基本単位による表し方
粘度	パスカル秒	Pa s	m^{-1} kg s^{-1}
力のモーメント	ニュートンメートル	N m	m^2 kg s^{-2}
表面張力	ニュートン毎メートル	N/m	kg s^{-2}
角速度	ラジアン毎秒	rad/s	m m^{-1} s^{-1}=s^{-1}
角加速度	ラジアン毎秒毎秒	rad/s^2	m m^{-1} s^{-2}=s^{-2}
熱流密度，放射照度	ワット毎平方メートル	W/m^2	kg s^{-3}
熱容量，エントロピー	ジュール毎ケルビン	J/K	m^2 kg s^{-2} K^{-1}
比熱容量，比エントロピー	ジュール毎キログラム毎ケルビン	J/(kg K)	m^2 s^{-2} K^{-1}
比エネルギー	ジュール毎キログラム	J/kg	m^2 s^{-2}
熱伝導率	ワット毎メートル毎ケルビン	W/(m K)	m kg s^{-3} K^{-1}
体積エネルギー	ジュール毎立方メートル	J/m^3	m^{-1} kg s^{-2}
電界の強さ	ボルト毎メートル	V/m	m kg s^{-3} A^{-1}
電荷密度	クーロン毎立方メートル	C/m^3	m^{-3} sA
表面電荷	クーロン毎平方メートル	C/m^2	m^{-2} sA
電束密度，電気変位	クーロン毎平方メートル	C/m^2	m^{-2} sA
誘電率	ファラド毎メートル	F/m	m^{-3} kg^{-1} s^4 A^2
透磁率	ヘンリー毎メートル	H/m	m kg s^{-2} A^{-2}
モルエネルギー	ジュール毎モル	J/mol	m^2 kg s^{-2} mol^{-1}
モルエントロピー, モル熱容量	ジュール毎モル毎ケルビン	J/(mol K)	m^2 kg s^{-2} K^{-1} mol^{-1}
照射線量（X線及びγ線）	クーロン毎キログラム	C/kg	kg^{-1} sA
吸収線量率	グレイ毎秒	Gy/s	m^2 s^{-3}
放射強度	ワット毎ステラジアン	W/sr	m^4 m^{-2} kg s^{-3}=m^2 kg s^{-3}
放射輝度	ワット毎平方メートル毎ステラジアン	$W/(m^2$ sr)	m^2 m^{-2} kg s^{-3}=kg s^{-3}
酵素活性濃度	カタール毎立方メートル	kat/m^3	m^{-3} s^{-1} mol

表５．SI 接頭語

乗数	接頭語	記号	乗数	接頭語	記号
10^{24}	ヨタ	Y	10^{-1}	デシ	d
10^{21}	ゼタ	Z	10^{-2}	センチ	c
10^{18}	エクサ	E	10^{-3}	ミリ	m
10^{15}	ペタ	P	10^{-6}	マイクロ	μ
10^{12}	テラ	T	10^{-9}	ナノ	n
10^9	ギガ	G	10^{-12}	ピコ	p
10^6	メガ	M	10^{-15}	フェムト	f
10^3	キロ	k	10^{-18}	アト	a
10^2	ヘクト	h	10^{-21}	ゼプト	z
10^1	デカ	da	10^{-24}	ヨクト	y

表６．SIに属さないが、SIと併用される単位

名称	記号	SI 単位による値
分	min	1 min=60s
時	h	1h =60 min=3600 s
日	d	1 d=24 h=86 400 s
度	°	1°=(π/180) rad
分	’	1’=(1/60)°=(π/10800) rad
秒	”	1”=(1/60)’=(π/648000) rad
ヘクタール	ha	$1ha=1hm^2=10^4m^2$
リットル	L, l	$1L=11=1dm^3=10^3cm^3=10^{-3}m^3$
トン	t	$1t=10^3$ kg

表７．SIに属さないが、SIと併用される単位で、SI単位で表される数値が実験的に得られるもの

名称	記号	SI 単位で表される数値
電子ボルト	eV	$1eV=1.602\ 176\ 53(14)\times10^{-19}J$
ダルトン	Da	$1Da=1.660\ 538\ 86(28)\times10^{-27}kg$
統一原子質量単位	u	1u=1 Da
天文単位	ua	$1ua=1.495\ 978\ 706\ 91(6)\times10^{11}m$

表８．SIに属さないが、SIと併用されるその他の単位

名称	記号	SI 単位で表される数値
バール	bar	1 bar=0.1MPa=100kPa=10^5Pa
水銀柱ミリメートル	mmHg	1mmHg=133.322Pa
オングストローム	Å	1 Å=0.1nm=100pm=10^{-10}m
海里	M	1 M=1852m
バーン	b	$1\ b=100fm^2=(10^{-12}cm)2=10^{-28}m^2$
ノット	kn	1 kn=(1852/3600)m/s
ネーパ	Np	SI単位との数値的な関係は、対数量の定義に依存。
ベル	B	
デジベル	dB	

表９．固有の名称をもつCGS組立単位

名称	記号	SI 単位で表される数値
エルグ	erg	$1\ erg=10^{-7}$ J
ダイン	dyn	$1\ dyn=10^{-5}$N
ポアズ	P	1 P=1 dyn s cm^{-2}=0.1Pa s
ストークス	St	1 St =$1cm^2$ s^{-1}=$10^{-4}m^2$ s^{-1}
スチルブ	sb	1 sb =1cd cm^{-2}=10^4cd m^{-2}
フォト	ph	1 ph=1cd sr cm^{-2} 10^4lx
ガル	Gal	1 Gal =1cm s^{-2}=$10^{-2}ms^{-2}$
マクスウェル	Mx	1 Mx = 1G cm^2=10^{-8}Wb
ガウス	G	1 G =1Mx cm^{-2} =10^{-4}T
エルステッド(c)	Oe	1 Oe≙ $(10^3/4\pi)$A m^{-1}

(c) ３元系のCGS単位系とSIでは直接比較できないため、等号「 ≙ 」は対応関係を示すものである。

表10．SIに属さないその他の単位の例

名称	記号	SI 単位で表される数値
キュリー	Ci	$1\ Ci=3.7\times10^{10}Bq$
レントゲン	R	$1\ R = 2.58\times10^{-4}C/kg$
ラド	rad	$1\ rad=1cGy=10^{-2}Gy$
レム	rem	$1\ rem=1\ cSv=10^{-2}Sv$
ガンマ	γ	1γ=1 nT=10-9T
フェルミ		1フェルミ=1 fm=10-15m
メートル系カラット		1メートル系カラット = 200 mg = 2×10-4kg
トル	Torr	1 Torr = (101 325/760) Pa
標準大気圧	atm	1 atm = 101 325 Pa
カロリー	cal	1cal=4.1858J（「15℃」カロリー），4.1868J（「IT」カロリー）4.184J（「熱化学」カロリー）
ミクロン	μ	1 μ =1μm=10^{-6}m

（第8版，2006年改訂）

この印刷物は再生紙を使用しています